SPECTRAL STABILITY OF IDEAL-GAS SHOCK LAYERS

JEFFREY HUMPHERYS, GREGORY LYNG, AND KEVIN ZUMBRUN

Abstract. Extending recent results in the isentropic case, we use a combination of asymptotic ODE estimates and numerical Evans-function computations to examine the spectral stability of shock-wave solutions of the compressible Navier–Stokes equations with ideal gas equation of state. Our main results are that, in appropriately rescaled coordinates, the Evans function associated with the linearized operator about the wave (i) converges in the large-amplitude limit to the Evans function for a limiting shock profile of the same equations, for which internal energy vanishes at one endstate; and (ii) has no unstable (positive real part) zeros outside a uniform ball $|\lambda| \leq \Lambda$. Thus, the rescaled eigenvalue ODE for the set of all shock waves, augmented with the (nonphysical) limiting case, form a compact family of boundary-value problems that can be conveniently investigated numerically. An extensive numerical Evans-function study yields one-dimensional spectral stability, independent of amplitude, for gas constant γ in $[1.2, 3]$ and ratio ν/μ of heat conduction to viscosity coefficient within $[0.2, 5]$ ($\gamma \approx 1.4$, $\nu/\mu \approx 1.47$ for air). Other values may be treated similarly but were not considered. The method of analysis extends also to the multi-dimensional case, a direction that we shall pursue in a future work.

Contents

Date: Last Updated: December 18, 2007.

J.H. was partially supported by NSF grant DMS-0607721. G.L. was partially supported by a Basic Research Grant from the College of Arts and Sciences at the University of Wyoming. K.Z. was partially supported by NSF grant DMS-0300487.

1. Introduction

A long-standing question in gas dynamics is the stability of viscous shock layers, or traveling-wave solutions

$$U(x,t) = \bar{U}(x-st), \quad \lim_{z\to\pm\infty} \bar{U}(z) = U_\pm,$$

of the compressible Navier–Stokes equations, where $U(x,t) = (v,u,E)^T$ is a vector recording specific volume, velocity, and total energy of the fluid at location $x \in \mathbb{R}$ and time $t \in \mathbb{R}^+$. A closely related question is the relation between Navier–Stokes solutions and solutions of the formally limiting Euler equations in the limit as viscosity and heat conduction coefficients go to zero: more precisely, validity of formal matched asymptotics predicting that the Navier–Stokes solution consists approximately of an Euler solution with smooth viscous shock layers replacing discontinuous Euler shocks.

Recent progress in the form of "Lyapunov-type" theorems established in [38, 54, 22, 23, 24] has reduced both problems to determination of spectral stability of shock layers, i.e., the study of the eigenvalue ODE associated with the linearized operator about the wave: a standard analytically and

numerically well-posed (boundary value) problem in ODE that can be attacked by the large body of techniques developed for asymptotic, exact, and numerical study of ODE. Indeed, the cited results hold for a substantially more general class of equations, and in one- or multi-dimensions.

In [29, 44, 15, 16], it has been established in a similarly general context (general equations, one- and multi-dimensions), using asymptotic ODE techniques, that spectral stability holds always in the small-amplitude limit, where amplitude is measured by $|U_+ - U_-|$, i.e., for shocks sufficiently close to a constant solution, thus satisfactorily resolving the long-time stability and small-viscosity limit problems for small-variation solutions.

However, until very recently, the spectral stability of *large-amplitude* shock waves has remained from a theoretical viewpoint essentially open, the sole exceptions being (i) a result of stability of Navier–Stokes shocks for isentropic gas dynamics with γ-law gas in the special case $\gamma \to 1$, obtained by Matsumura-Nishihara [39] quite early on using an ingenious energy estimate specific to that case; and (ii) and a result of Zumbrun [55]—again obtained by energy estimates special to the model—which establishes the stability of stationary phase-transitional shocks of an isentropic viscous-capillary van der Waals model introduced by Slemrod [49].

Progress instead has focused, quite successfully, on the development of efficient and general numerical methods for the study of stability of individual waves, or compact families of waves, of essentially arbitrary systems; see, for example, [6, 7, 8, 5, 30, 4]. These techniques, based on Evans-function computations, effectively resolve the question of spectral stability for waves of large but finite amplitude, but leave open the question of stability in the large-amplitude limit. For discussion of the Evans function and its numerical computation, see [1, 17, 54, 8, 4] or Section 3.4 below.

Quite recently, however, Humpherys, Lafitte, and Zumbrun [27] have introduced a new strategy combining asymptotic ODE techniques with numerical Evans-function computations, by which they were able to carry out a global analysis of shock stability in the isentropic γ-law case, yielding stability independent of amplitude for $\gamma \in [1, 2.5]$.[1] Specifically, after an appropriate rescaling, they showed by a detailed asymptotic analysis of the linearized eigenvalue ODE that the associated Evans functions (determining stability of the viscous shock profile) converge in the large-amplitude limit to an Evans function associated with their formal limit, which may then be studied either numerically or analytically (for example, by energy estimate as in [27]).

The purpose of the present paper is to extend the approach of [27] to the full (nonisentropic) Navier–Stokes equations of compressible gas dynamics with ideal gas equation of state, resolving in this fundamental case the long-standing questions of viscous shock stability and behavior in the small-viscosity limit. Specifically, we show, as in the isentropic case, that the

[1]Other γ may be treated similarly but were not considered.

Evans function indeed converges in the large-amplitude limit, to a value corresponding to the Evans function of a limiting system. Compactifying the parameter range by adjoining this limiting system, we then carry out systematic numerical Evans-function computations as in [4, 27] to determine stability for gas constant $\gamma \in [1.2, 3]$ and (rescaled) ratio of heat conduction to viscosity coefficient $\nu/\mu \in [0.2, 5]$, well-including the physical values given in Appendices A and B. The result, as in the isentropic case, is *unconditional stability, independent of amplitude for an ideal gas equation of state.*

1.1. **Discussion and open problems.** The asymptotic analysis of [27] is quite delicate; it depends sensitively both on the use of Lagrangian coordinates and on the precise way of writing the eigenvalue ODE as a first-order system. It is thus not immediately clear that the analysis can be extended to the more complicated nonisentropic case. Moreover, since Lagrangian coordinates—specifically, the associated change of spatial variable

$$\mathrm{d}\tilde{x}/\mathrm{d}x = \rho(x), \tag{1.1}$$

where ρ is density—are not available in multi-dimensions, it is likewise, at first glance, unclear how how to extend the analysis beyond one spatial dimension.

Remarkably, we find that the structure of the full, physical equations is much more favorable to the analysis than that of the isentropic model. In particular, whereas in the isentropic case the eigenvalue equations in the large-amplitude limit are a nonstandard singular perturbation of the limiting equations that must be analyzed "by hand", in the full (nonisentropic) gas case, they are a *regular perturbation* for which convergence may be concluded by standard theorems on continuous dependence of the Evans function with respect to parameters; see, for example, the basic convergence lemma of [44].

Indeed, for γ bounded away from the nonphysical case $\gamma = 1$ (see Section 2 for a description of the equations and the physical background), we have the striking difference that, for a fixed left endstate U_-, the density remains uniformly bounded above and below for all viscous shock profiles connecting U_- to a right state U_+, with energy going to infinity in the large-amplitude limit. By contrast, in the isentropic case, the density is artificially tied to energy and thus density goes to infinity in the large-amplitude limit for any $\gamma \geq 1$; see, e.g., [46, 47, 48]. This untangling of the large-amplitude behaviors of the density and the energy sets the stage for our analysis. Below, to see this untangling, instead of fixing a left endstate U_- and asking which right endstates U_+ may be connected to U_- by a viscous shock profile, we fix the shock speed $s = -1$ and all coordinates of the left state U_- *except* the energy. We find again that the density stays bounded above and below for all possible right states U_+ connected by a shock profile to some such U_-.

Since the equations remain regular so long as density is bounded from zero and infinity, one important consequence of this fact is that we need only

check a few basic properties such as uniform decay of profiles and continuous extension of stable/unstable subspaces to conclude that the strong-shock limit is in the nonisentropic case a regular perturbation of the limiting system as claimed; see Section 3 for details.

A second important consequence is that Lagrangian and Eulerian coordinates are essentially equivalent in the nonisentropic case so long as γ remains uniformly bounded from 1, whereas, in the isentropic case, the equations become singular for Eulerian (x) coordinates in the large-amplitude limit, by (1.1) together with the fact that density goes to infinity. Here, we have chosen to work with Lagrangian coordinates for comparison with previous one-dimensional analyses in the isentropic case [4, 27, 12]. However, we could just as well have worked in Eulerian coordinates, including full multi-dimensional effects, to obtain by the same arguments that the large-amplitude limit is a regular perturbation of the (unintegrated) limiting eigenvalue equation, and therefore the Evans functions converge in the limit also in this multi-dimensional setting.

Likewise, uniform bounds on unstable eigenvalues may be obtained in multi-dimensions by adapting the asymptotic analysis of [22] similarly as we have adapted in Section 4 the asymptotic analysis of [37]. Thus, for γ uniformly bounded from 1, *the analysis of this paper extends with suitable modification to the multi-dimensional case*, making possible the resolution of multi-dimensional viscous stability by a systematic numerical Evans-function study as in the one-dimensional case. We shall carry out the multi-dimensional analysis in a following work [28].

Presumably, the same procedure of compactifying the parameter space after rescaling to bounded domain would work for any gas law with appropriate asymptotic behavior as $\rho, e \to \infty$. Thus, we could in principle investigate also van der Waals gas/fluids, for example, which could yield interesting different behavior: in particular, (as known already from stability index considerations [57, 54]) instability in some regimes. Other interesting areas for investigation include the study of boundary layer stability (see [12] for an analysis of the isentropic case), and stability of weak and strong detonation solutions (analogous to shock waves) of the compressible Navier–Stokes equations for a reacting gas. A further interesting direction is to investigate the effects of temperature dependence of viscosity and heat conduction on behavior for large amplitudes; see Appendices B.2 and F.

In this work, we have restricted to the parameter range $\gamma \in [1.2, 3]$ and $\nu/\mu \in [0.2, 5]$, where γ is the gas constant, $\nu = \kappa/c_v$ is a rescaled coefficient of heat conduction (κ the Fourier conduction and c_v specific heat), and μ is the coefficient of viscosity; see equations. (2.1)–(2.3), Section 2. Similar computations may be carried out for arbitrary γ bounded away from the nonphysical limit $\gamma = 1$. To approach the singular limit $\gamma = 1$ would presumably require a nonstandard singular perturbation analysis like that of [27] in the isentropic case, as the structure is similar; see Remark 2.2. The limits $\nu/\mu \to 0$ and $\nu/\mu \to \infty$ are more standard singular perturbations with

fast/slow structure that should be treatable by the methods of [1]; this would be a very interesting direction for further study. We note that our results for large ν/μ do indicate possible further simplification in behavior, as the singular perturbation structure would suggest; see Remark 4.8 and Figure 4. For dry air at normal temperatures, $\gamma \approx 1.4$ and $\nu/\mu \approx 1.47$, well within range; see Appendix A.

Finally, we mention the issue of rigorous verification. Our results, though based on rigorous analysis, do not constitute numerical proof, and are not intended to. In particular, we do not use interval arithmetic. Nonetheless, the numerical evidence for stability appears overwhelming, particularly in view of the fact that the family $\{D(\lambda, v_+)\}$ of Evans contours estimated in the stability computations is analytic in both parameters, yielding extremely strong interpolation estimates by the rigidity of analytic functions.

In any case, our analysis contains all of the elements necessary for numerical proof, the effective realization of which, however, is a separate problem of independent interest. Given the fundamental nature of the problem, we view this as an important area for further investigation.

1.2. **Plan of the paper.** In Section 2, we set up the problem, describing the equations, rescaling appropriately, and verifying existence and uniform decay of profiles independent of shock strength. In Section 3, we construct the Evans function and establish the key fact that it is continuous in all parameters up to the strong-shock limit. In Section 4, we carry out the main technical work of the paper, establishing an upper bound on the modulus of unstable eigenvalues of the linearized operator about the wave in terms of numerically approximable quantities associated with the traveling-wave profile. In Section 5, we describe our numerical method, first estimating a maximal radius within which unstable eigenvalues are confined, then computing the winding number of the Evans function around the semicircle with that radius to estimate the number of unstable eigenvalues, for (a discretization of) all parameters within the compact parameter domain, including the strong-shock limit. Finally, in Section 6, we perform the numerical computations indicating stability.

In Appendices A and B, we discuss further the dimensionless constants Γ and ν/μ, and determine their values for air and other common gases. In Appendix C, we discuss equations of state for fluids and dense gases. In Appendix D, we compute a formula for the Mach number, a useful dimensionless quantity measuring shock strength independent of scaling. In Appendix E, we give a general bound on the operator norm of lifted matrices acting on exterior products, useful for analysis of the exterior product method of [6, 5]. In Appendix F, we discuss the changes needed to accommodate temperature-dependence in the coefficients of viscosity and heat conduction, as predicted by the kinetic theory of gases.

2. Preliminaries

In Lagrangian coordinates, the Navier–Stokes equations for compressible gas dynamics take the form

$$v_t - u_x = 0, \tag{2.1}$$

$$u_t + p_x = \left(\frac{\mu u_x}{v}\right)_x, \tag{2.2}$$

$$E_t + (pu)_x = \left(\frac{\mu u u_x}{v}\right)_x + \left(\frac{\kappa T_x}{v}\right)_x, \tag{2.3}$$

where v is the specific volume, u is the velocity, p is the pressure, and the energy E is made up of the internal energy e and the kinetic energy:

$$E = e + \frac{u^2}{2}. \tag{2.4}$$

The constants μ and κ represent viscosity and heat conductivity. Finally, T is the temperature, and we assume that the internal energy e and the pressure p are known functions of the specific volume and the temperature:

$$p = p_0(v, T), \quad e = e_0(v, T).$$

An important special case occurs when we consider an ideal, polytropic gas. In this case the energy and pressure functions take the specific form

$$p_0(v, T) = \frac{\bar{R}T}{v}, \quad e_0(v, T) = c_v T, \tag{2.5}$$

where $\bar{R} > 0$ and $c_v > 0$ are constants that characterize the gas. Alternatively, the pressure may be written as

$$p = \frac{\Gamma e}{v}, \tag{2.6}$$

where $\Gamma = \gamma - 1 = \frac{\bar{R}}{c_v} > 0$, $\gamma > 1$ the adiabatic index. Equivalently, in terms of the entropy and specific volume, the pressure reads

$$p(v, S) = a e^{S/c_v} v^{-\gamma},$$

where S is thermodynamical entropy, or $p(v) = a v^{-\gamma}$ in the isentropic approximation; see [46, 4, 27].

In the thermodynamical rarefied gas approximation, $\gamma > 1$ is the average over constituent particles of $\gamma = (N + 2)/N$, where N is the number of internal degrees of freedom of an individual particle, or, for molecules with "tree" (as opposed to ring, or other more complicated) structure,

$$\gamma = \frac{2n + 3}{2n + 1}, \tag{2.7}$$

where n is the number of constituent atoms [3]: $\gamma = 5/3 \approx 1.66$ for monatomic, $\gamma = 7/5 = 1.4$ for diatomic gas. For fluids or dense gases, γ is typically determined phenomenologically [26]. In general, γ is usually taken within $1 \leq \gamma \leq 3$ in models of gas-dynamical flow, whether phenomenological or derived by statistical mechanics [46, 47, 48].

2.1. **Viscous shock profiles.** A *viscous shock profile* of (2.1)–(2.3) is a traveling-wave solution,

$$v(x,t) = \hat{v}(x-st), \;\; u(x,t) = \hat{u}(x-st), \;\; T(x,t) = \hat{T}(x-st), \tag{2.8}$$

moving with speed s and connecting constant states $(v_\pm, u_\pm, T_\pm)$. Such a solution is a stationary solution of the system of PDEs

$$v_t - sv_x - u_x = 0, \tag{2.9}$$

$$u_t - su_x + p_0(v,T)_x = \left(\frac{\mu u_x}{v}\right)_x, \tag{2.10}$$

(2.11)

$$\big[e_0(v,T)+u^2/2\big]_t - s\big[e_0(v,T)+u^2/2\big]_x + (p_0(v,T)u)_x = \left(\frac{\mu u u_x}{v}\right)_x + \left(\frac{\kappa T_x}{v}\right)_x.$$

2.2. **Rescaled equations.** Under the rescaling

$$(x,t,v,u,T) \to (-\epsilon s x, \epsilon s^2 t, v/\epsilon, -u/(\epsilon s), T/(\epsilon^2 s^2)), \tag{2.12}$$

where ϵ is chosen so that $v_- = 1$, the system (2.9)-(2.11) becomes

$$v_t + v_x - u_x = 0, \tag{2.13}$$

$$u_t + u_x + p_x = \left(\frac{\mu u_x}{v}\right)_x, \tag{2.14}$$

$$E_t + E_x + (pu)_x = \left(\frac{\mu u u_x}{v}\right)_x + \left(\frac{\kappa T_x}{v}\right)_x, \tag{2.15}$$

where the pressure and internal energy in the (new) rescaled variables are given by

$$p(v,T) = \epsilon^{-1} s^{-2} p_0(\epsilon v, \epsilon^2 s^2 T) \tag{2.16}$$

and

$$e(v,T) = \epsilon^{-2} s^{-2} e_0(\epsilon v, \epsilon^2 s^2 T); \tag{2.17}$$

in the ideal gas case, *the pressure and internal energy laws remain unchanged*

$$p(v,T) = \frac{\bar{R}T}{v}, \qquad e(v,T) = c_v T, \tag{2.18}$$

with the same $\bar{R}$, c_v. Likewise, Γ remains unchanged in (2.6).

2.3. **Rescaled profile equations.** Viscous shock profiles of (2.13)–(2.15) satisfy the system of ordinary differential equations

$$v' - u' = 0, \tag{2.19}$$

$$u' + p(v,T)' = \left(\frac{\mu u'}{v}\right)', \tag{2.20}$$

$$\big[e(v,T) + u^2/2\big]' + (p(v,T)u)' = \left(\frac{\mu u u'}{v}\right)' + \left(\frac{\kappa T'}{v}\right)', \tag{2.21}$$

together with the boundary conditions

$$\big(v(\pm\infty), u(\pm\infty), T(\pm\infty)\big) = \big(v_\pm, u_\pm, T_\pm\big).$$

Evidently, we can integrate each of the differential equations from $-\infty$ to x, and using the boundary conditions (in particular $v_- = 1$ and $u_- = 0$), we find, after some elementary manipulations, the profile equations:

(2.22)

$$\mu v' = v\Big[(v-1) + p(v,T) - p(v_-,T_-)\Big],$$

(2.23)

$$\kappa T' = v\left[e(v,T) + \frac{(v-1)^2}{2} - e(v_-,T_-)\right] + v(v-1)\Big[p(v_-,T_-) - (v-1)\Big].$$

We note that in the case of an ideal gas, with $v_- = 1$, these ODEs simplify somewhat, to

$$v' = \frac{1}{\mu}\left[v(v-1) + \Gamma(e - ve_-)\right], \tag{2.24}$$

$$e' = \frac{v}{\nu}\left[-\frac{(v-1)^2}{2} + (e - e_-) + (v-1)\Gamma e_-\right]. \tag{2.25}$$

where $\nu := \kappa/c_v$ and Γ is as in (2.6).

Remark 2.1. *Remarkably, the right-hand sides of the profile ODE are polynomial in (v, e), so smooth even for values on the boundaries $\hat{v} = 0$ or $\hat{e} = 0$ of the physical parameter range. This is in sharp contrast to the isentropic case* [4, 27]*, for which the ODE become singular as $v \to 0$, except in the special case $\gamma = 1$.*

2.4. **Rankine-Hugoniot conditions.** Substituting v_+, u_+, e_+ into the rescaled profile equations (2.19)–(2.21) and requiring that the right-hand side vanish yields the Rankine-Hugoniot conditions

$$-s[v] = [u], \tag{2.26}$$

$$-s[u] = -[p], \tag{2.27}$$

$$-s\left[e + \frac{u^2}{2}\right] = -[pu], \tag{2.28}$$

where $[f(U)] := f(U_+) - f(U_-)$ denotes jump between $U_\pm$.

We specialize now to the ideal gas case. Under the scaling (2.12), we have $s = -1$, $v_- = 1$, $u_- = 0$. Fixing $\Gamma_{max} \geq \Gamma \geq \Gamma_{min} > 0$ and letting v_+ vary in the range $1 \geq v_+ \geq v_*(\Gamma) := \Gamma/(\Gamma+2)$, we use (2.26)–(2.28) to solve for

$$u_+, e_+ \text{ and } e_-.$$

Our assumptions reduce (2.26)–(2.28) to

$$v_+ - 1 = u_+, \tag{2.29}$$

$$u_+ = -(p_+ - p_-) = -\Gamma\Big(\frac{e_+}{v_+} - e_-\Big), \tag{2.30}$$

$$(e_+ - e_-) + \frac{u_+^2}{2} = -p_+u_+ = -\Gamma\frac{e_+u_+}{v_+}. \tag{2.31}$$

Equation (2.29) immediately gives u_+. Subtracting $\frac{u_+}{2}$ times (2.30) from (2.31), and rearranging, we obtain

$$e_+ = e_-\frac{1+\frac{\Gamma}{2}(1-v_+)}{1-\frac{\Gamma}{2v_+}(1-v_+)} = \frac{e_-v_+}{(\Gamma+2)}\frac{(\Gamma+2-\Gamma v_+))}{(v_+-v_*)}, \tag{2.32}$$

$v_* = \frac{\Gamma}{\Gamma+2}$, from which we obtain the physicality condition

$$v_+ > v_* := \frac{\Gamma}{\Gamma+2}, \tag{2.33}$$

corresponding to positivity of the denominator, with $\frac{e_+}{e_-} \to +\infty$ as $v \to v_*$. Finally, substituting into $1 = s^2 = -\frac{[p]}{[v]}$ and rearranging, we obtain

$$e_- = \frac{(\Gamma+2)(v_+-v_*)}{2\Gamma(\Gamma+1)}, \tag{2.34}$$

and thus

$$e_+ = \frac{v_+(\Gamma+2-\Gamma v_+)}{2\Gamma(\Gamma+1)}, \tag{2.35}$$

completing the description of the endstates.

We see from this analysis that the strong-shock limit corresponds, for fixed Γ, to the limit $v_+ \to v_*$, with all other parameters functions of v_+. In this limit,

$$v_- = 1, \quad u_- = 0, \quad e_- \sim (v_+ - v_*) \to 0, \tag{2.36}$$

and

$$u_+ \sim (v_+ - 1) \to \frac{-2}{\Gamma+2}, \quad e_+ \to \frac{1-v_*^2}{2(\Gamma+1)} = \frac{2}{(\Gamma+2)^2}. \tag{2.37}$$

At this point, taking without loss of generality $\mu = 1$, we have reduced to a three-parameter family of problems on compact parameter range, parametrized by $\Gamma_{max} \geq \Gamma \geq \Gamma_{min} > 0$, $1 \geq v_+ \geq v_*(\Gamma) \geq v_*(\Gamma_{min}) > 0$, and $\nu_{max} \geq \nu \geq \nu_{min}$.

Remark 2.2. *As $\Gamma \to 0$, we find from (2.35) that e_+ blows up as $(v_+ - v_*)/\Gamma$, i.e., our rescaled coordinates remain bounded only if $v_+ - v_* \leq C\Gamma \to 0$, $C > 0$ constant, as well. (This is reflected in the limiting profile equation for $\Gamma = 0$, which admits only profiles from $v_- = 1$ to $v_+ = 0$; see (2.25), which, for $\Gamma = 0$, reduces to $v' = v(v-1)$.) Thus, our techniques apply for $\Gamma \to 0$ only in the (simultaneous) large-amplitude limit.*

2.5. **Existence and decay of profiles.** Specializing to the ideal gas case, we next study existence and behavior of profiles. Existence and exponential decay of profiles has been established by Gilbarg [21] for all *finite-amplitude shocks* $1 \geq v_+ > v_*$. Thus, the question is whether these properties extend to the strong-shock limit, the main issue being to establish *uniform exponential decay* as $x \to \pm\infty$, independent of shock strength.

Since the profile equations (2.24)–(2.25) are smooth (polynomial) in (v, e), the issue of uniform decay reduces essentially to *uniform hyperbolicity* of end-states $(v, e)_\pm$, i.e., nonexistence of purely imaginary linearized growth/decay rates at $\pm\infty$. Linearizing (2.24)–(2.25) about an equilibrium state, we obtain

$$\begin{pmatrix} v \\ e \end{pmatrix}' = M \begin{pmatrix} v \\ e \end{pmatrix}, \qquad M := \begin{pmatrix} \mu^{-1} & 0 \\ 0 & v\nu^{-1} \end{pmatrix} \begin{pmatrix} 2v - 1 - \Gamma e_- & \Gamma \\ 1 - v + \Gamma e_- & 1 \end{pmatrix}. \tag{2.38}$$

Since M is 2×2, its eigenvalues are

$$m = \frac{\mathrm{tr}M \pm \sqrt{\mathrm{tr}M^2 - 4 \det M}}{2},$$

and so hyperbolicity is equivalent to $\det M \neq 0$ and $\det M < 0$ or $\mathrm{tr}M \neq 0$.

Computing, we have

$$\det M = (v/\mu\nu)\Big((\Gamma + 2)v - (\Gamma + 1)(1 + \Gamma e_-)\Big), \tag{2.39}$$

so that $\det M \gtrless 0$ is equivalent (for $\Gamma > 0$, hence $v \geq v_* > 0$) to

$$(\Gamma + 2)v - (\Gamma + 1)(1 + \Gamma e_-) \gtrless 0. \tag{2.40}$$

At $v = v_- = 1$, this reduces to $e_- \neq \frac{1}{\Gamma(\Gamma+1)}$, or, using (2.34) to

$$v_+ \frac{(\Gamma + 2)(1 - v_+)}{2} > 0,$$

except in the characteristic case $v_+ = 1$, while

$$\mathrm{tr}M = \mu^{-1}(1 - \Gamma e_- + (\nu/\mu)^{-1}) \geq \mu^{-1}(1 - \frac{\Gamma + 2}{2(\Gamma + 1)} + (\nu/\mu)^{-1}) \geq \nu > 0.$$

At $v = v_+$, (2.40) reduces, using (2.34), to

$$\det M = (v_+/\mu\nu)\Big(v_+ \frac{(\Gamma + 2)(v_+ - 1)}{2}\Big) < 0,$$

except in the characteristic case $v_+ = 1$. Thus, for v_+ bounded from zero, *hyperbolicity fails at* $x = \pm\infty$ *only in the characteristic case* $v_- = v_+ = 1$.

Next, let us recall the existence proof of [21], which proceeds by the observation that isoclines $v' = 0$ and $e' = 0$ obtained by setting the right-hand sides of (2.24) and (2.25) to zero bound a convex lens-shaped region whose vertices are the unique equilibria $U_\pm$, that is invariant under the forward flow of (2.24)–(2.25), and into which enters the unstable manifold of U_-; recall that $\det M < 0$ at $-\infty$, hence there is a one-dimensional unstable manifold. It follows that the unstable manifold must approach attractor U_+ as $x \to +\infty$, determining the unique connecting orbit describing the profile.

By the above-demonstrated hyperbolicity, this argument extends also to the case $v_+ = v_*$ ($e_- = 0$), yielding at once existence and uniform boundedness of profiles across the whole parameter range (recall that $(v,e)_\pm$ are uniformly bounded, by the Rankine–Hugoniot analysis of the previous section), in particular for the limiting profile equations at $v_+ = v_*$ of

$$v' = \frac{1}{\mu}\left[v(v-1) + \Gamma e\right], \tag{2.41}$$

$$e' = \frac{v}{\nu}\left[-\frac{(v-1)^2}{2} + e\right]. \tag{2.42}$$

Collecting facts, we have the following key result.

Lemma 2.3. *For Γ bounded and bounded away from the nonphysical limit $\Gamma = 0$, μ, ν bounded and bounded from zero, and v_+ bounded away from the characteristic limit $v_- = 1$, profiles $\hat U = (\hat v, \hat u, \hat e)^T$ of the rescaled equations (2.24)–(2.25) exist for all $1 \geq v_+ \geq v_*$, decaying exponentially to their endstates $U_\pm$ as $x \to \pm\infty$, uniformly in Γ, v_+, μ, ν.*

Proof. Existence, boundedness, and exponential decay of individual profiles follow from the discussion above. Uniform bounds follow by smooth dependence on parameters together with compactness of the parameter range. □

3. Evans function formulation

From now on, we specialize to the ideal gas case, setting without loss of generality $\mu = 1$.

3.1. **Linearized integrated eigenvalue equations.** Defining integrated variables

$$\tilde v := \int_{-\infty}^x v\,dy, \quad \tilde u := \int_{-\infty}^x u\,dy, \quad \tilde E := \int_{-\infty}^x E\,dy,$$

we note that the rescaled equations (2.13)– (2.15) can be written in terms of the integrated variables in the form

$$\begin{aligned} \tilde v_t + \tilde v_x - \tilde u_x &= 0, \\ \tilde u_t + \tilde u_x + \frac{\Gamma(\tilde E_x - \frac{\tilde u_x^2}{2})}{\tilde v_x} &= \frac{\tilde u_{xx}}{\tilde v_x}, \\ \tilde E_t + \tilde E_x + \frac{\Gamma \tilde u_x(\tilde E_x - \frac{\tilde u_x^2}{2})}{\tilde v_x} &= \frac{\tilde u_x \tilde u_{xx}}{\tilde v_x} + \frac{\nu(\tilde E_x - \frac{\tilde u_x^2}{2})_x}{\tilde v_x}. \end{aligned} \tag{3.1}$$

The integrated viscous profile,

$$\tilde{\hat v} := \int_{-\infty}^x \hat v\,dy, \quad \tilde{\hat u} := \int_{-\infty}^x \hat u\,dy, \quad \tilde{\hat E} := \int_{-\infty}^x \hat E\,dy,$$

is a stationary solution of (3.1). Then we write

$$\tilde v = \tilde{\hat v} + v, \quad \tilde u = \tilde{\hat u} + u, \quad \tilde E = \tilde{\hat E} + E,$$

and we linearize (3.1) about the integrated profile. By an abuse of notation, we denote the perturbation by v, u, and E. Note also that the integrated profile always appears under an x-derivative; this explains the appearance of "hats" in place of "tilde-hats" in the expression below. Finally, we use the relationship $\hat{E} = \hat{e} - \frac{\hat{u}^2}{2}$ to simplify some of the expressions. We obtain the linearized integrated equations

(3.2)
$$\begin{aligned} v_t + v_x - u_x &= 0, \\ u_t + u_x + \frac{\Gamma(E_x - \hat{u}u_x)}{\hat{v}} - \frac{\Gamma\hat{e}}{\hat{v}^2}v_x &= \frac{u_{xx}}{\hat{v}} - \frac{\hat{u}_x}{\hat{v}^2}v_x, \\ E_t + E_x + \frac{\Gamma\hat{u}(E_x - \hat{u}u_x)}{\hat{v}} + \frac{\Gamma\hat{e}}{\hat{v}}u_x - \frac{\Gamma\hat{e}\hat{u}}{\hat{v}^2}v_x &= \frac{\hat{u}u_{xx}}{\hat{v}} + \frac{\hat{u}_x}{\hat{v}}u_x - \frac{\hat{u}\hat{u}_x}{\hat{v}^2}v_x \\ &\quad + \frac{\nu(E_x - \hat{u}u_x)_x}{\hat{v}} - \frac{\nu\hat{e}_x}{\hat{v}^2}v_x. \end{aligned}$$

Defining $\epsilon := E - \hat{u}u$, subtracting $\hat{u}$ times the second equation from the third, and rearranging, we obtain, finally, the linearized integrated eigenvalue equations:

(3.3)
$$\begin{aligned} &\lambda v + v' - u' = 0, \\ &\lambda u + u' + \frac{\Gamma}{\hat{v}}\epsilon' + \frac{\Gamma\hat{u}_x}{\hat{v}}u + \left[-\frac{\Gamma\hat{e}}{\hat{v}^2} + \frac{\hat{u}_x}{\hat{v}^2}\right]v' = \frac{u''}{\hat{v}}, \\ &\lambda\epsilon + \epsilon' + \left[\hat{u}_x - \frac{\nu\hat{u}_{xx}}{\hat{v}}\right]u + \left[\frac{\Gamma\hat{e}}{\hat{v}} - (\nu+1)\frac{\hat{u}_x}{\hat{v}}\right]u' + \left[\frac{\nu\hat{e}_x}{\hat{v}^2}\right]v' = \frac{\nu}{\hat{v}}\epsilon''. \end{aligned}$$

3.2. **Expression as a first-order system.** Following [4], we may express (3.3) concisely as a first-order system

$$W' = A(x,\lambda)W, \tag{3.4}$$

$$A(x,\lambda) = \begin{pmatrix} 0 & 1 & 0 & 0 & 0 \\ \lambda\nu^{-1}\hat{v} & \nu^{-1}\hat{v} & \nu^{-1}\hat{v}\hat{u}_x - \hat{u}_{xx} & \lambda g(\hat{U}) & g(\hat{U}) - h(\hat{U}) \\ 0 & 0 & 0 & \lambda & 1 \\ 0 & 0 & 0 & 0 & 1 \\ 0 & \Gamma & \lambda\hat{v} + \Gamma\hat{u}_x & \lambda\hat{v} & f(\hat{U}) - \lambda \end{pmatrix}, \tag{3.5}$$

$$W = (\epsilon, \epsilon', u, v, v')^T, \quad {}' = \frac{\mathrm{d}}{\mathrm{d}x}, \tag{3.6}$$

where, using $\hat{u}_x = \hat{v}_x$ and (2.24) with $\mu = 1$,

$$\begin{aligned} g(\hat{U}) &:= \nu^{-1}(\Gamma\hat{e} - (\nu+1)\hat{u}_x) \\ &= \nu^{-1}\Gamma\hat{e} - -\frac{\nu+1}{\nu}\hat{v}_x \\ &= \nu^{-1}\Gamma\hat{e} - \frac{\nu+1}{\nu}\Big(\hat{v}(\hat{v}-1) + \Gamma(\hat{e} - \hat{v}e_-)\Big) \end{aligned} \tag{3.7}$$

$$f(\hat{U}) := \frac{\hat{u}_x - \Gamma\hat{e}}{\hat{v}} + \hat{v} = 2\hat{v} - 1 - \Gamma e_-. \tag{3.8}$$

$$h(\hat{U}) := -\frac{\hat{e}_x}{\hat{v}} = -\nu^{-1}\left(-\frac{(\hat{v}-1)^2}{2} + (\hat{e} - e_-) + (\hat{v}-1)\Gamma e_-\right). \tag{3.9}$$

Remark 3.1. *Remarkably, similarly as for the profile equations, the entries of A are polynomial in $(\hat{v}, \hat{u}, \hat{e})$. Thus, both profile and linearized eigenvalue equations are perfectly well-behaved for any compact subset of $\Gamma > 0$.*

3.3. **Consistent splitting.** Denote by $A_\pm(\lambda) := \lim_{x\to\pm\infty} A(x,\lambda)$ the limiting coefficient matrices at $x = \pm\infty$. (These limits exist by exponential convergence of profiles $\hat{U}$, Lemma 2.3.) Denote by $S_\pm$ and $U_\pm$ the stable and unstable subspaces of $A_\pm$.

Definition 3.2. *Following* [1]*, we say that* (3.4) *exhibits consistent splitting on a given λ-domain if $A_\pm$ are hyperbolic, with* $\dim S_+$ *and* $\dim U_-$ *constant and summing to the dimension of the full space (in this case* 5*).*

By analytic dependence of A on λ and standard matrix perturbation theory, S^+ and U_- are analytic on any domain for which consistent splitting holds.

Lemma 3.3. *For all $\Gamma > 0$, $1 \geq v_+ > v_*$,* (3.4)–(3.5) *exhibit consistent splitting on $\{\Re\lambda \geq 0\} \setminus \{0\}$, with* $\dim S_+ = 3$ *and* $\dim U_- = 2$*. Moreover, subspaces S_+ and U_-, along with their associated spectral projections, extend analytically in λ and continuously in Γ, ν, v_-, to $\{\Re\lambda \geq 0\}$ for $\Gamma > 0$, $\nu > 0$, and $1 > v_+ \geq v_*$.*

Proof. Consistent splitting and analytic extension to $\lambda = 0$ follow by the general results of [37], except at the strong-shock limit $v_+ = v_*$, where

$$A_-^*(\lambda) = \begin{pmatrix} 0 & 1 & 0 & 0 & 0 \\ \lambda\nu^{-1} & \nu^{-1} & 0 & 0 & 0 \\ 0 & 0 & 0 & \lambda & 1 \\ 0 & 0 & 0 & 0 & 1 \\ 0 & \Gamma & \lambda & \lambda & 1-\lambda \end{pmatrix} \tag{3.10}$$

and

$$A_+^*(\lambda) = \begin{pmatrix} 0 & 1 & 0 & 0 & 0 \\ \lambda\nu^{-1}v_* & \nu^{-1}v_* & 0 & \lambda g(U_+) & g(U_+) \\ 0 & 0 & 0 & \lambda & 1 \\ 0 & 0 & 0 & 0 & 1 \\ 0 & \Gamma & \lambda v_* & \lambda v_* & f(U_+) - \lambda \end{pmatrix}, \tag{3.11}$$

where $g(U_+) = \frac{(1-v_*)}{\nu}(v_* - (\nu - 1))$ and $f(U_+) = \frac{\Gamma-2}{\Gamma+2}$.

The matrix A_-^* is lower block-triangular, with diagonal blocks

$$\begin{pmatrix} 0 & 1 \\ \lambda\nu^{-1} & \nu^{-1} \end{pmatrix}, \qquad \begin{pmatrix} 0 & \lambda & 1 \\ 0 & 0 & 1 \\ \lambda & \lambda & 1-\lambda \end{pmatrix}$$

corresponding respectively to the scalar convection-diffusion equation

$$e_t + e_x = \nu e_{xx}$$

and the isentropic case treated in [27], The first has eigenvalues $\mu = \frac{1\pm\sqrt{1+4\lambda}}{2}$, so satisfies consistent splitting on $\{\Re\lambda \geq 0\}\setminus\{0\}$, with analytic continuation (since eigenvalues remain separated) to $\Re\lambda \geq 0$. The second, as observed in [27], has eigenvalues $\mu = -\lambda, \frac{1\pm\sqrt{1+4\lambda}}{2}$, hence likewise satisfies consistent splitting on $\{\Re\lambda \geq 0\}\setminus\{0\}$ and (since the single unstable eigenvalue remains separated from the two stable eigenvalues) continues analytically to $\Re\lambda \geq 0$. Indeed, the unstable manifold has dimension two for all $\Re\lambda \geq 0$, hence is analytic on that domain. This verifies the proposition at $x = -\infty$ by direct calculation.

At $x = +\infty$, the computation is more difficult. Here, we refer instead to the abstract results of [37], which assert that hyperbolic–parabolic systems of the type treated here, including the limiting case, at least for $v_* \neq 0$, exhibit consistent splitting on $\{\Re\lambda \geq 0\} \setminus \{0\}$, with analytic extension to $\Re\lambda \geq 0$, so long as the shock is noncharacteristic, i.e., the flux Jacobian associated with the first-order part of the equations have nonvanishing determinants at $x = \pm\infty$. These may be computed in any coordinates, in particular (v, u, ϵ). Neglecting terms originating from diffusion, i.e., including only first-order terms from the left-hand side, we obtain from (3.3) the flux Jacobian

$$\begin{pmatrix} 1 & -1 & 0 \\ -\Gamma e/v^2 & 1 & \Gamma/v \\ 0 & \Gamma e/v & 1 \end{pmatrix},$$

which has determinant $\Delta = 1 - \Gamma^2 e/v^2 - \Gamma e/v^2$, giving for $v_+ = v_*$ ($e_- = 0$) that $\Delta_{-\infty} = 1 > 0$ and, calculating at $v_+ = v_*$ that

$$\Gamma e_+/v_*^2 = 2, \quad \Delta_{+\infty} = -1 - 2\Gamma < 0.$$

Thus, we may conclude by the general results of [37] that consistent splitting holds at both $x = \pm\infty$ on $\{\Re\lambda \geq 0\} \setminus \{0\}$ for $1 \geq v_+ \geq v_*$, with analytic extension to $\Re\lambda \geq 0$. □

Remark 3.4. *We note that the results of* [37] *do not apply at $x = -\infty$, $v_+ = v_*$, where $e_- = 0$ leaves the physical domain. Specifically, at this value the genuine coupling condition of Kawashima* [34]*, hence the dissipativity condition of* [37] *fails, and so we cannot conclude consistent splitting; indeed, the eigenvalue $\mu \equiv \lambda$ (corresponding to the decoupled hyperbolic mode) is pure imaginary for any pure imaginary λ.*

3.4. **Construction of the Evans function.** We now construct the Evans function associated with (3.4)–(3.5), following the approach of [37, 44].

Lemma 3.5. *There exist bases $V^- = (V_1^-, V_2^-)(\lambda)$, $V^+ = (V_3^+, V_4^+, V_5^+)(\lambda)$ of $U_-(\lambda)$ and $S_+(\lambda)$, extending analytically in λ and continuously in Γ, ν, v_- to $\{\Re\lambda \geq 0\}$ for $\Gamma > 0$, $\nu > 0$, and $1 > v_+ \geq v_*$, determined by Kato's ODE*

$$V' = (PP' - P'P)V, \tag{3.12}$$

where P denotes the spectral projection onto S_+, U_-, respectively, and $'$ denotes $d/d\lambda$.

Proof. This follows from Lemma 3.3 by a standard result of Kato [33], valid on any simply connected set in λ on which P remains analytic. □

Lemma 3.6. *There exist bases*

$$W^- = (W_1^-, W_2^-)(\lambda), \quad W^+ = (W_3^+, W_4^+, W_5^+)(\lambda)$$

of the unstable manifold at $-\infty$ and the stable manifold at $x = +\infty$ of (3.4)–(3.5)*, asymptotic to $e^{A_- x}V^-$ and $e^{A_+ x}V^+$, respectively, as $x \to \mp\infty$, and extending analytically in λ and continuously in Γ, ν, v_+ to $\{\Re\lambda \geq 0\}$ for $\Gamma > 0$, $\nu > 0$, and $1 > v_+ \geq v_*$.*

Proof. This follows, using the conjugation lemma of [40], by uniform exponential convergence of A to $A_\pm$ as $x \to \pm\infty$, Lemma 2.3. □

Definition 3.7. *The Evans function associated with* (3.4)–(3.5) *is defined as*

$$D(\lambda) := \det(W^+, W^-)|_{x=0}. \tag{3.13}$$

Proposition 3.8. *The Evans function $D(\cdot)$ is analytic in λ and continuous in Γ, ν, v_+ on $\Re\lambda \geq 0$ and $\Gamma > 0$, $\nu > 0$, and $1 > v_+ \geq v_*$. Moreover, on $\{\Re\lambda \geq 0\} \setminus \{0\}$, its zeros correspond in location and multiplicity with eigenvalues of the integrated linearized operator $\mathcal{L}$, or, equivalently with solutions of* (3.3) *decaying at $x = \pm\infty$.*

Proof. The first statement follows by Lemma 3.6, the second by a standard result of Gardner and Jones [18, 19], valid on the region of consistent splitting. □

Remark 3.9. *Proposition 3.8 includes in passing the key information that the Evans function converges in the strong-shock limit $v_+ \to v_*$ to the Evans function for the limiting system at $v_+ = v_*$, uniformly on compact subsets of $\{\Re\lambda \geq 0\}$, as illustrated numerically in Fig. 6.*

Remark 3.10. *The specification in* (3.12) *of initializing bases at infinity is optimal in that it minimizes "action" in a certain sense; see* [31] *for further discussion. In particular,* for any constant-coefficient system, the Evans function induced by Kato bases (3.12) is identically constant in λ. *For, in this case, bases W^+ and W^- are given at $x = 0$ by the values $V^\pm$ prescribed in* (3.12)*, and both evolve according to the same ODE, hence $W = (W^-, W^+)_{x=0}$ satisfies $W' = [P, P']W$ and $D(\lambda) := \det W \equiv$ constant by Abel's Theorem and the fact that $\operatorname{tr}[P, P'] = 0$, where $[P, P'] := PP' - P'P$.*

Remark 3.11. *More generally,* $\det(V^-, V^+) \equiv$ constant *in the "traveling pulse" case $U_+ = U_-$, by the argument of Remark 3.10, whence the Evans function constructed here may be seen to agree with the "natural" Evans*

function (independent of the choice of $V^\pm$)

$$E(\lambda) := \frac{\det(W^+, W^-)|_{x=0}}{\det(V^+, V^-)} = \frac{\tilde W^+ \cdot W^-|_{x=0}}{\tilde V^+ \cdot V^-} \tag{3.14}$$

defined in [43] *for that case. The latter may in turn be seen to agree with a (*2*-modified) characteristic Fredholm determinant of the associated linearized operator L about the wave* [20]*, formally equivalent to*

$$\det_2(I + (L_0 - \lambda)^{-1}(L - L_0)) \sim \frac{\det_2(L - \lambda)}{\det_2(L_0 - \lambda)},$$

where L_0 denotes the (constant-coefficient) linearized operator about the background state $U_\pm$. Our construction by Kato's ODE thus gives a natural extension to the traveling-front case of the canonical constructions of [43, 20] in the traveling-pulse case*, neither of which generalizes in obvious fashion to the traveling-front setting (the difficulty in both cases coming from the fact that* $\det(V^+, V_-)$ *may vanish).*

4. High-frequency bounds

We now carry out the main technical work of the paper, establishing the following uniform bounds on the size of unstable eigenvalues.

Proposition 4.1. *Nonstable eigenvalues λ of* (3.3)*, i.e., eigenvalues with nonnegative real part, are confined for $\gamma > 1$, $v_* < v_+ \le 1$ to a finite region $|\lambda| \le \Lambda$, for any*

$$\Lambda \ge 2\max\{1, \nu\} \max_x \Big(\frac{|\mathcal{F}^*_{--}| + |\mathcal{F}^*_{++}| + 2\sqrt{|\mathcal{F}^*_{-+}||\mathcal{F}^*_{+-}|}}{\hat v^{1/2}}(x, \Lambda) \Big)^2, \tag{4.1}$$

where

$$|\mathcal{F}^*_{kl}|(x, \Lambda) := \sum_{i=0}^4 \frac{|\mathcal{F}_{-i/2,kl}|}{|\Lambda|^{i/2}}(x), \tag{4.2}$$

$k, l = +, -$, $\mathcal{F}_{j,kl}$ are as defined in (4.22) *below, and $|\cdot|$ is the matrix operator norm with respect to any specified norm on $\mathbb{C}^5$.*

Before establishing Proposition 4.1, we give a general discussion indicating the ideas behind the proof. For $v_+ > v_*$, such high-frequency bounds have already been established by asymptotic ODE estimates in [37]. For $v_+ = v_*$, the problem leaves the class studied in [37] (specifically, the dissipativity condition is neutrally violated as discussed in Remark 3.4), hence requires further discussion.

However, a brief examination reveals that the argument of [37] applies in this case almost unchanged. For, recall that the method of [37] to obtain high-frequency bounds was to decompose the flow of the first-order eigenvalue equation for high frequencies into parabolic growth and decay modes of equal dimensions $r = \dim(u, e)$ with growth rates $\Re\mu \sim \pm|\lambda|^{1/2}$, and hyperbolic modes of dimension $n - r$, in the present case $\dim v = 1$, with growth

rate $\sim \pm(\Re\lambda + 1)$ up to an exponentially decaying error term $\sim e^{-\theta|x|}$, the delicate point being to separate decaying from growing hyperbolic modes.

In the present, degenerate case, the hyperbolic rates are only $\sim \Re\lambda$ plus decaying error term, and so the final, delicate part of the argument in [37] does not apply. However, since there is only a single hyperbolic mode, this part of the argument is not needed. Specifically, the $|\lambda|^{1/2}/C$ spectral gap between parabolic and hyperbolic modes allow us for high frequencies to decompose the flow of the eigenvalue equation into the direct sum of growing parabolic modes blowing up exponentially at $x = +\infty$, decaying parabolic modes blowing up exponentially at $-\infty$, and a single hyperbolic mode that blows up exponentially at $-\infty$ for $v_+ > v_*$ and, though it does not blow up exponentially for $v_+ = v_*$, is in any case always transverse to the unstable manifold at $x = -\infty$.

To put things another way, the unstable manifold at $x = -\infty$ consists for $|\lambda|$ sufficiently large precisely of growing parabolic modes, which blow up at $x = +\infty$. Thus, there exist no zeros of the Evans function, since these correspond to solutions belonging to both the unstable manifold at $-\infty$ and the stable (hence decaying) manifold at $+\infty$. This shows the existence of uniform high-frequency bounds- it remains to establish quantitative bounds by keeping track of constants throughout the argument.

Remark 4.2. *A review of the above shows that the same argument applies whenever hyperbolic modes are uniformly decaying or growing, i.e., in the situation identified in* [38, 54, 22] *that all hyperbolic characteristic speeds have a common sign. Likewise, the multidimensional case may be treated by essentially the same argument, following the generalization given in* [22].

Proof of Proposition 4.1. We carry out the argument in two steps.

1. Preparation. Recasting (3.4), (3.5) in the standard coordinates of [37], as

$$Z' = B(x,\lambda)Z, \quad Z = (v, u, \epsilon, u', \epsilon')^T, \tag{4.3}$$

(4.4)

$$B(x,\lambda) = \begin{pmatrix} -\lambda & 0 & 0 & 1 & 0 \\ 0 & 0 & 0 & 1 & 0 \\ 0 & 0 & 0 & 0 & 1 \\ \lambda(f(\hat{U}) - \hat{v}) & \lambda\hat{v} + \Gamma\hat{u}_x & 0 & f(\hat{U}) & \Gamma \\ \lambda h(\hat{U}) & \nu^{-1}\hat{v}\hat{u}_x - \hat{u}_{xx} & \lambda\nu^{-1}\hat{v} & g(\hat{U}) - h(\hat{U}) & \nu^{-1}\hat{v} \end{pmatrix},$$

and we decompose B as $B = \lambda B_1 + B_0$ with

$$B_1(x) = \begin{pmatrix} -1 & 0 & 0 & 0 & 0 \\ 0 & 0 & 0 & 0 & 0 \\ 0 & 0 & 0 & 0 & 0 \\ f(\hat{U}) - \hat{v} & \hat{v} & 0 & 0 & 0 \\ h(\hat{U}) & 0 & \nu^{-1}\hat{v} & 0 & 0 \end{pmatrix}, \tag{4.5}$$

and

$$B_0(x) = \begin{pmatrix} 0 & 0 & 0 & 1 & 0 \\ 0 & 0 & 0 & 1 & 0 \\ 0 & 0 & 0 & 0 & 1 \\ 0 & \Gamma\hat{u}_x & 0 & f(\hat{U}) & \Gamma \\ 0 & \nu^{-1}\hat{v}\hat{u}_x - \hat{u}_{xx} & 0 & g(\hat{U}) - h(\hat{U}) & \nu^{-1}\hat{v} \end{pmatrix}. \tag{4.6}$$

Noting that B_1 is lower block-triangular, with (1×1) upper diagonal block -1 strictly negative, and (4×4) lower diagonal block

$$\alpha := \begin{pmatrix} 0 & 0 & 0 & 0 \\ 0 & 0 & 0 & 0 \\ \hat{v} & 0 & 0 & 0 \\ 0 & \nu^{-1}\hat{v} & 0 & 0 \end{pmatrix},$$

having all zero eigenvalues, we block-diagonalize by the lower block-diagonal transformation $Z := T\mathcal{X}$,

$$T := \begin{pmatrix} 1 & 0 \\ \theta & I_4 \end{pmatrix}, \quad T^{-1} := \begin{pmatrix} 1 & 0 \\ -\theta & I_4 \end{pmatrix},$$

$$\theta := -(\alpha + I_4)^{-1} \begin{pmatrix} 0 \\ 0 \\ f(\hat{U}) - \hat{v} \\ h(\hat{U}) \end{pmatrix},$$

where, since $\alpha^2 = 0$, $(I + \alpha)^{-1} = I - \alpha$, hence

$$\theta = -\begin{pmatrix} 0 \\ 0 \\ f(\hat{U}) - \hat{v} \\ h(\hat{U}) \end{pmatrix} + \alpha \begin{pmatrix} 0 \\ 0 \\ f(\hat{U}) - \hat{v} \\ h(\hat{U}) \end{pmatrix} = \begin{pmatrix} 0 \\ 0 \\ -f(\hat{U}) + \hat{v} \\ -h(\hat{U}) \end{pmatrix},$$

and

$$T^{-1}T' = \begin{pmatrix} 0 & 0 \\ \theta' & 0 \end{pmatrix} = \begin{pmatrix} 0 & 0 & 0 & 0 & 0 \\ 0 & 0 & 0 & 0 & 0 \\ 0 & 0 & 0 & 0 & 0 \\ -\hat{v}_x & 0 & 0 & 0 & 0 \\ j(\hat{U}) & 0 & 0 & 0 & 0 \end{pmatrix},$$

$j(\hat{U}) := \nu^{-1}\Big((\Gamma e_- - (\hat{v} - 1))\hat{v}_x + \hat{e}_x\Big)$, to obtain $\mathcal{X}' = C\mathcal{X}$,

$$C = T^{-1}BT - T^{-1}T' = \lambda C_1 + C_0,$$

where

$$C_1(x,\lambda) = \begin{pmatrix} -1 & 0 & 0 & 0 & 0 \\ 0 & 0 & 0 & 0 & 0 \\ 0 & 0 & 0 & 0 & 0 \\ 0 & \hat{v} & 0 & 0 & 0 \\ 0 & 0 & \nu^{-1}\hat{v} & 0 & 0 \end{pmatrix}, \tag{4.7}$$

is in a variant of block Jordan form and

$$C_0(x,\lambda) = \begin{pmatrix} \hat v - f(\hat U) & 0 & 0 & 1 & 0 \\ \hat v - f(\hat U) & 0 & 0 & 1 & 0 \\ -h(\hat U) & 0 & 0 & 0 & 1 \\ k(\hat U) & \Gamma \hat u_x & 0 & 2f(\hat U) - \hat v & \Gamma \\ l(\hat U) & \nu^{-1}\hat v \hat u_x - \hat u_{xx} & 0 & g(\hat U) & \nu^{-1}\hat v \end{pmatrix}, \tag{4.8}$$

where

$$\begin{aligned} k(\hat U) &:= (2f(\hat U) - \hat v)(\hat v - f(\hat U)) - \Gamma h(\hat U) + \hat v_x, \\ l(\hat U) &:= g(\hat U)(\hat v - f(\hat U)) - \nu^{-1}\hat v h(\hat U) - j(\hat U). \end{aligned} \tag{4.9}$$

Making the further transformation $\mathcal{X} = Q\mathcal{Y}$,

$$Q := \begin{pmatrix} 1 & \beta \\ 0 & I_4 \end{pmatrix}, \quad Q^{-1} := \begin{pmatrix} 1 & -\beta \\ 0 & I_4 \end{pmatrix},$$

$$\begin{aligned} \beta &:= \lambda^{-1}(0,0,1,0)(I_4 + \alpha)^{-1} \\ &= \lambda^{-1}(0,0,1,0)(I_4 - \alpha) \\ &= \lambda^{-1}(-\hat v, 0, 1, 0), \end{aligned}$$

$$Q^{-1}Q' = \begin{pmatrix} 0 & \beta' \\ 0 & 0 \end{pmatrix} = \lambda^{-1} \begin{pmatrix} 0 & -\hat v_x & 0 & 0 & 0 \\ 0 & 0 & 0 & 0 & 0 \\ 0 & 0 & 0 & 0 & 0 \\ 0 & 0 & 0 & 0 & 0 \\ 0 & 0 & 0 & 0 & 0 \end{pmatrix},$$

we obtain $\mathcal{Y}' = D\mathcal{Y}$,

$$\begin{aligned} D &= Q^{-1}CQ - Q^{-1}Q' \\ &= \lambda D_1 + D_0 + \lambda^{-1}D_{-1} + \lambda^{-2}D_{-2}, \end{aligned}$$

where $D_1 = C_1$,

$$D_0(x,\lambda) = \begin{pmatrix} \hat v - f(\hat U) & 0 & 0 & 0 & 0 \\ \hat v - f(\hat U) & 0 & 0 & 1 & 0 \\ -h(\hat U) & 0 & 0 & 0 & 1 \\ k(\hat U) & \Gamma \hat u_x & 0 & 2f(\hat U) - \hat v & \Gamma \\ l(\hat U) & \nu^{-1}\hat v \hat u_x - \hat u_{xx} & 0 & g(\hat U) & \nu^{-1}\hat v \end{pmatrix}, \tag{4.10}$$

(4.11)

$$D_{-1}(x,\lambda) = \begin{pmatrix} m(\hat U) & -\hat v^2 + f(\hat U)\hat v - \Gamma \hat u_x + \hat v_x & 0 & 3(\hat v - f(\hat U)) & -\Gamma \\ 0 & -\hat v(\hat v - f(\hat U)) & 0 & \hat v - f(\hat U) & 0 \\ 0 & -\hat v h(\hat U) & 0 & -h(\hat U) & 0 \\ 0 & -\hat v k(\hat U) & 0 & k(\hat U) & 0 \\ 0 & -\hat v l(\hat U) & 0 & l(\hat U) & 0 \end{pmatrix},$$

and

$$D_{-2}(x,\lambda) = \begin{pmatrix} 0 & -\hat{v}m(\hat{U}) & 0 & m(\hat{U}) & 0 \\ 0 & 0 & 0 & 0 & 0 \\ 0 & 0 & 0 & 0 & 0 \\ 0 & 0 & 0 & 0 & 0 \\ 0 & 0 & 0 & 0 & 0 \end{pmatrix}, \tag{4.12}$$

where

$$m(\hat{U}) := \hat{v}(\hat{v} - f(\hat{U})) - k(\hat{U}).$$

Making the "balancing" transformation $\mathcal{Y} = V\mathcal{Z}$, $V = \begin{pmatrix} I_3 & 0 \\ 0 & \lambda^{1/2} I_2 \end{pmatrix}$, we then obtain $\mathcal{Z}' = E\mathcal{Z}$, $E = V^{-1}DV$, where

$$E = \begin{pmatrix} -\lambda & 0 & 0 & 0 & 0 \\ 0 & 0 & 0 & \lambda^{1/2} & 0 \\ 0 & 0 & 0 & 0 & \lambda^{1/2} \\ 0 & \lambda^{1/2}\hat{v} & 0 & 0 & 0 \\ 0 & 0 & \lambda^{1/2}\nu^{-1}\hat{v} & 0 & 0 \end{pmatrix} + \Theta, \tag{4.13}$$

$$\Theta = \Theta_0 + \lambda^{-1/2}\Theta_{-1/2} + \lambda^{-1}\Theta_{-1} + \lambda^{-3/2}\Theta_{-3/2} + \lambda^{-2}\Theta_{-2},$$

where

$$\Theta_0(x) = \begin{pmatrix} \hat{v} - f(\hat{U}) & 0 & 0 & 0 & 0 \\ \hat{v} - f(\hat{U}) & 0 & 0 & 0 & 0 \\ -h(\hat{U}) & 0 & 0 & 0 & 0 \\ 0 & 0 & 0 & 2f(\hat{U}) - \hat{v} & \Gamma \\ 0 & 0 & 0 & g(\hat{U}) & \nu^{-1}\hat{v} \end{pmatrix}, \tag{4.14}$$

$$\Theta_{-1/2}(x) = \begin{pmatrix} 0 & 0 & 0 & 3(\hat{v} - f(\hat{U})) & -\Gamma \\ 0 & 0 & 0 & \hat{v} - f(\hat{U}) & 0 \\ 0 & 0 & 0 & -h(\hat{U}) & 0 \\ k(\hat{U}) & \Gamma\hat{u}_x & 0 & 0 & 0 \\ l(\hat{U}) & \nu^{-1}\hat{v}\hat{u}_x - \hat{u}_{xx} & 0 & 0 & 0 \end{pmatrix}, \tag{4.15}$$

$$\Theta_{-1}(x) = \begin{pmatrix} m(\hat{U}) & -\hat{v}(\hat{v} - f(\hat{U})) + \hat{v}_x - \Gamma\hat{u}_x & 0 & 0 & 0 \\ 0 & -\hat{v}(\hat{v} - f(\hat{U}) & 0 & 0 & 0 \\ 0 & \hat{v}h(\hat{U}) & 0 & 0 & 0 \\ 0 & 0 & 0 & k(\hat{U}) & 0 \\ 0 & 0 & 0 & l(\hat{U}) & 0 \end{pmatrix}, \tag{4.16}$$

$$\Theta_{-3/2}(x) = \begin{pmatrix} 0 & 0 & 0 & m(\hat{U}) & 0 \\ 0 & 0 & 0 & 0 & 0 \\ 0 & 0 & 0 & 0 & 0 \\ 0 & -\hat{v}k(\hat{U}) & 0 & 0 & 0 \\ 0 & -\hat{v}l(\hat{U}) & 0 & 0 & 0 \end{pmatrix}, \tag{4.17}$$

$$\Theta_{-2}(x) = \begin{pmatrix} 0 & -\hat{v}m(\hat{U}) & 0 & 0 & 0 \\ 0 & 0 & 0 & 0 & 0 \\ 0 & 0 & 0 & 0 & 0 \\ 0 & 0 & 0 & 0 & 0 \\ 0 & 0 & 0 & 0 & 0 \end{pmatrix}. \tag{4.18}$$

Finally, setting $\mathcal{Z} = \tilde{S}X$, with

$$\tilde{S} := \begin{pmatrix} 1 & 0 \\ 0 & \tilde{s} \end{pmatrix}, \quad \tilde{s} := \begin{pmatrix} I & I \\ -A & A \end{pmatrix}, \quad \tilde{s}^{-1} := \frac{1}{2}\begin{pmatrix} I & -A^{-1} \\ I & A^{-1} \end{pmatrix},$$

$$A := \begin{pmatrix} \sqrt{\hat{v}} & 0 \\ 0 & \sqrt{\nu^{-1}\hat{v}} \end{pmatrix}, \quad A^{-1} := \begin{pmatrix} 1/\sqrt{\hat{v}} & 0 \\ 0 & 1/\sqrt{\nu^{-1}\hat{v}} \end{pmatrix},$$

$$\tilde{S}^{-1}\tilde{S}_x = \begin{pmatrix} 0 & 0 \\ 0 & \tilde{s}^{-1}\tilde{s}_x \end{pmatrix} \quad \tilde{s}^{-1}\tilde{s}_x = (\hat{v}_x/4\hat{v}) \begin{pmatrix} I & -I \\ -I & I \end{pmatrix},$$

we obtain

$$X' = (F + \mathcal{F})X, \tag{4.19}$$

where

$$F = \tilde{S}^{-1}E\tilde{S} = \begin{pmatrix} M_- & 0 \\ 0 & M_+ \end{pmatrix} \tag{4.20}$$

with

$$M_+ := \begin{pmatrix} \lambda^{1/2}\hat{v}^{1/2} & 0 \\ 0 & \lambda^{1/2}(\hat{v}/\nu)^{1/2} \end{pmatrix}, \tag{4.21}$$

$$M_- := \begin{pmatrix} -\lambda & 0 & 0 \\ 0 & -\lambda^{1/2}\hat{v}^{1/2} & 0 \\ 0 & 0 & -\lambda^{1/2}(\hat{v}/\nu)^{1/2} \end{pmatrix},$$

and

$$\begin{aligned} \mathcal{F} &= \tilde{S}^{-1}\Theta\tilde{S} - \tilde{S}^{-1}\tilde{S}_x \\ &= \mathcal{F}_0 + \lambda^{-1/2}\mathcal{F}_{-1/2} + \lambda^{-1}\mathcal{F}_{-1} + \lambda^{-3/2}\mathcal{F}_{-3/2} + \lambda^{-2}\mathcal{F}_{-2}, \end{aligned} \tag{4.22}$$

where

$$\mathcal{F}_0(x) = \tag{4.23}$$

$$\begin{pmatrix} \hat{v} - f(\hat{U}) & 0 & 0 & 0 & 0 \\ \frac{\hat{v}-f(\hat{U})}{2} & \frac{2f(\hat{U})-\hat{v}}{2} - \frac{\hat{v}_x}{4\hat{v}} & \frac{\sqrt{\nu^{-1}}\Gamma}{2} & -\frac{2f(\hat{U})-\hat{v}}{2} + \frac{\hat{v}_x}{4\hat{v}} & \frac{-\sqrt{1/\nu}\Gamma}{2} \\ \frac{-h(\hat{U})}{2} & \frac{g(\hat{U})}{2\sqrt{1/\nu}} & \frac{\nu^{-1}\hat{v}}{2} - \frac{\hat{v}_x}{4} & -\frac{g(\hat{U})}{2\sqrt{1/\nu}} & -\frac{\nu^{-1}\hat{v}}{2} + \frac{\hat{v}_x}{4} \\ \frac{\hat{v}-f(\hat{U})}{2} & -\frac{2f(\hat{U})-\hat{v}}{2} + \frac{\hat{v}_x}{4\hat{v}} & -\frac{\sqrt{1/\nu}\Gamma}{2} & \frac{2f(\hat{U})-\hat{v}}{2} - \frac{\hat{v}_x}{4\hat{v}} & \frac{\sqrt{1/\nu}\Gamma}{2} \\ \frac{-h(\hat{U})}{2} & -\frac{g(\hat{U})}{2\sqrt{1/\nu}} & -\frac{\nu^{-1}\hat{v}}{2} + \frac{\hat{v}_x}{4} & \frac{g(\hat{U})}{2\sqrt{1/\nu}} & \frac{\nu^{-1}\hat{v}}{2} - \frac{\hat{v}_x}{4} \end{pmatrix},$$

(4.24) $\mathcal{F}_{-1/2}(x) =$

$$\begin{pmatrix} 0 & -3\sqrt{\hat v}(\hat v - f(\hat U)) & \Gamma\sqrt{\frac{\hat v}{\nu}} & 3\sqrt{\hat v}(\hat v - f(\hat U)) & -\Gamma\sqrt{\frac{\hat v}{\nu}} \\ \frac{-k(\hat U)}{2\sqrt{\hat v}} & \frac{-\Gamma\hat u_x}{2\sqrt{\hat v}} - \frac{\sqrt{\hat v}}{2}(\hat v - f(\hat U)) & 0 & \frac{-\Gamma\hat u_x}{2\sqrt{\hat v}} + \frac{\sqrt{\hat v}}{2}(\hat v - f(\hat U)) & 0 \\ \frac{-l(\hat U)}{2\sqrt{\hat v/\nu}} & -\frac{n(\hat U)}{2\sqrt{\nu^{-1}\hat v}} + \frac{h(\hat U)\sqrt{\hat v}}{2} & 0 & -\frac{n(\hat U)}{2\sqrt{\nu^{-1}\hat v}} - \frac{h(\hat U)\sqrt{\hat v}}{2} & 0 \\ \frac{k(\hat U)}{2\sqrt{\hat v}} & \frac{\Gamma\hat u_x}{2\sqrt{\hat v}} - \frac{\sqrt{\hat v}}{2}(\hat v - f(\hat U)) & 0 & \frac{\Gamma\hat u_x}{2\sqrt{\hat v}} + \frac{\sqrt{\hat v}}{2}(\hat v - f(\hat U)) & 0 \\ \frac{l(\hat U)}{2\sqrt{\hat v/\nu}} & \frac{n(\hat U)}{2\sqrt{\hat v/\nu}} + \frac{h(\hat U)\sqrt{\hat v}}{2} & 0 & \frac{n(\hat U)}{2\sqrt{\hat v/\nu}} - \frac{h(\hat U)\sqrt{\hat v}}{2} & 0 \end{pmatrix},$$

$$n(\hat U) := \nu^{-1}\hat v\hat u_x - \hat u_{xx},$$

(4.25) $$\mathcal{F}_{-1}(x) = \begin{pmatrix} m(\hat U) & q(\hat U) & 0 & q(\hat U) & 0 \\ 0 & \frac{-\hat v(\hat v - f(\hat U)) + k(\hat U)}{2} & 0 & \frac{-\hat v(\hat v - f(\hat U)) - k(\hat U)}{2} & 0 \\ 0 & \frac{\hat v h(\hat U)}{2} + \frac{l(\hat U)}{2\sqrt{\nu^{-1}}} & 0 & \frac{\hat v h(\hat U)}{2} - \frac{l(\hat U)}{2\sqrt{\nu^{-1}}} & 0 \\ 0 & \frac{-\hat v(\hat v - f(\hat U)) - k(\hat U)}{2} & 0 & \frac{-\hat v(\hat v - f(\hat U)) + k(\hat U)}{2} & 0 \\ 0 & \frac{\hat v h(\hat U)}{2} - \frac{l(\hat U)}{2\sqrt{\nu^{-1}}} & 0 & \frac{\hat v h(\hat U)}{2} + \frac{l(\hat U)}{2\sqrt{\nu^{-1}}} & 0 \end{pmatrix},$$

(4.26) $$q(\hat U) := -\hat v(\hat v - f(\hat U)) - \Gamma\hat u_x + \hat v_x,$$

(4.27) $$\mathcal{F}_{-3/2}(x) = \begin{pmatrix} 0 & -\hat v^{1/2} m(\hat U) & 0 & \hat v^{1/2} m(\hat U) & 0 \\ 0 & \frac{\hat v^{1/2} k(\hat U)}{2} & 0 & \frac{\hat v^{1/2} k(\hat U)}{2} & 0 \\ 0 & \frac{\hat v^{1/2} l(\hat U)}{2\sqrt{\nu^{-1}}} & 0 & \frac{\hat v^{1/2} l(\hat U)}{2\sqrt{\nu^{-1}}} & 0 \\ 0 & -\frac{\hat v^{1/2} k(\hat U)}{2} & 0 & \frac{-\hat v^{1/2} k(\hat U)}{2} & 0 \\ 0 & -\frac{\hat v^{1/2} l(\hat U)}{2\sqrt{\nu^{-1}}} & 0 & -\frac{\hat v^{1/2} l(\hat U)}{2\sqrt{\nu^{-1}}} & 0 \end{pmatrix},$$

(4.28) $$\mathcal{F}_{-2}(x) = \begin{pmatrix} 0 & -\hat v m(\hat U) & 0 & -\hat v m(\hat U) & 0 \\ 0 & 0 & 0 & 0 & 0 \\ 0 & 0 & 0 & 0 & 0 \\ 0 & 0 & 0 & 0 & 0 \\ 0 & 0 & 0 & 0 & 0 \end{pmatrix}.$$

2. Tracking. Denoting $X_- = (X_1, X_2, X_3)^T$, $X_+ = (X_4, X_5)^T$, and

$$\mathcal{F} = \begin{pmatrix} \mathcal{F}_{--} & \mathcal{F}_{-+} \\ \mathcal{F}_{+-} & \mathcal{F}_{++} \end{pmatrix},$$

we obtain from (4.19)–(4.20)

(4.29) $$\begin{aligned} &|X_-|' \le |\mathcal{F}_{--}||X_-| + |\mathcal{F}_{-+}||X_+|, \\ &|X_+|' \ge \min\{1, \nu^{-1/2}\}\hat v^{1/2}\Re\lambda^{1/2}|X_+| - |\mathcal{F}_{+-}||X_-| - |\mathcal{F}_{++}||X_+|, \end{aligned}$$

from which, defining $\zeta := |X_-|/|X_+|$, we obtain by a straightforward computation the Ricatti equation

$$\zeta' \leq \Big(-\min\{1,\nu^{-1/2}\}\hat{v}^{1/2}\Re\lambda^{1/2}+|\mathcal{F}_{--}|+|\mathcal{F}_{++}|\Big)\zeta+|\mathcal{F}_{-+}|+|\mathcal{F}_{+-}|\zeta^2. \tag{4.30}$$

Denote by

$$\begin{aligned}\zeta_\pm := &\frac{\min\{1,\nu^{-1/2}\}\hat{v}^{1/2}\Re\lambda^{1/2}-|\mathcal{F}_{--}|-|\mathcal{F}_{++}|}{2|\mathcal{F}_{+-}|}\\ &\pm\sqrt{\Big(\frac{\min\{1,\nu^{-1/2}\}\hat{v}^{1/2}\Re\lambda^{1/2}-|\mathcal{F}_{--}|-|\mathcal{F}_{++}|}{2|\mathcal{F}_{+-}|}\Big)^2-\frac{|\mathcal{F}_{-+}|}{|\mathcal{F}_{+-}|}}\end{aligned} \tag{4.31}$$

the roots of

$$\Big(-\min\{1,\nu^{-1/2}\}\hat{v}^{1/2}\Re\lambda^{1/2}+|\mathcal{F}_{--}|+|\mathcal{F}_{++}|\Big)\zeta+|\mathcal{F}_{-+}|+|\mathcal{F}_{+-}|\zeta^2=0. \tag{4.32}$$

Assuming for all x the condition

$$\max\{1,\nu^{1/2}\}\frac{|\mathcal{F}_{--}|+|\mathcal{F}_{++}|+2\sqrt{|\mathcal{F}_{-+}||\mathcal{F}_{+-}|}}{\hat{v}^{1/2}}<\Re\lambda^{1/2}, \tag{4.33}$$

$\zeta_\pm$ are positive real and distinct, whence, consulting (4.30), we see that $\zeta'<0$ on the interval $\zeta_-<\zeta<\zeta_+$.

It follows that $\Omega_- := \{\zeta\leq\zeta_-\}$ is an invariant region under the forward flow of (4.19); moreover, this region is exponentially attracting for $\zeta<\zeta_+$. A symmetric argument yields that $\Omega_+ := \{\zeta\geq\zeta_+\}$ is invariant under the backward flow of (4.19), and exponentially attracting for $\zeta>\zeta_-$. Specializing these observations to the constant-coefficient limiting systems at $x=-\infty$ and $x=+\infty$, we find that the invariant subspaces of the limiting coefficient matrices from which the Evans function is constructed must lie in Ω_- and Ω_+, respectively. By forward (respectively. backward) invariance of Ω_- (respectively. Ω_+), under the full, variable-coefficient flow, we thus find that the manifold Span W^- of solutions initiated at $x=-\infty$ in the construction of the Evans function lies in Ω_- for all x, while the manifold Span W^+ of solutions initiated at $x=+\infty$ lies in Ω_+ for all x.

Since Ω_- and Ω_+ are distinct, we may conclude that under condition (4.33), Span W^+ and Span W^- are transverse and the Evans function does not vanish. But (4.1) implies (4.33), by $\Re\lambda^{1/2}\geq\frac{|\lambda|^{1/2}}{\sqrt{2}}$ together with (4.22). □

4.1. **Universality and convergence in the high-frequency limit.** The bounds obtaining from (4.1) may in practice be rather conservative, as illustrated by the following example.

Example 4.3. *For the constant-coefficient scalar operator* $L := \partial_x^2 - a\partial_x$, *write* $(L-\lambda)w=0$ *as a first-order system* $W'=(A+\Theta)W$, $W=(w,w'/\lambda^{1/2})^T$, *where* $A=\lambda^{1/2}\begin{pmatrix}0&1\\1&0\end{pmatrix}$, $\Theta=\begin{pmatrix}0&0\\0&a\end{pmatrix}$. *Block-diagonalizing* A *by* $W=$

RZ, $R = \begin{pmatrix} 1 & 1 \\ 1 & -1 \end{pmatrix}$, we obtain $Z' = (\tilde{A} + \tilde{\Theta})Z$, where $\tilde{A} = \mathrm{diag}(1, -1)$, $\tilde{\Theta} = R^{-1}\Theta R = (a/2)\begin{pmatrix} 1 & -1 \\ -1 & 1 \end{pmatrix}$. Applying the analog of (4.33) on $\Re\lambda \geq 0$, where $\delta = 2\Re\lambda^{1/2} \geq |\lambda|^{1/2}$, we obtain nonexistence of eigenvalues for $|\lambda|^{1/2} \geq 2|a|$, giving eigenbound $|\lambda| \leq 4|a|^2$. By contrast, standard elliptic energy estimates give $|\lambda| \leq |a|^2/4$, which, by direct Fourier transform computation, is optimal. Comparing, we see that the tracking bound is of the correct order, $O(|a|^2)$, but with coefficient 16 times larger than optimal.

This simple calculation may explain the ratio of roughly 10 between the nonisentropic bounds found by tracking in Section 5.2 and the isentropic energy bounds found in [4, 27]. The following result may be used to gauge at a practical level the efficiency of the analytical tracking bounds by a (nonrigorous, but typically quite sharp) numerical convergence study.

Proposition 4.4. *On the nonstable half-plane $\Re\lambda \geq 0$,*

$$\lim_{|\lambda|\to\infty} D(\lambda)/e^{\alpha\lambda^{1/2}} = \text{constant}, \tag{4.34}$$

(4.35)

$$\alpha := (1 + \nu^{-1/2})\left(\int_{-\infty}^{0} (\hat{v}^{1/2}(x) - v_-^{1/2})\,\mathrm{d}x + \int_{0}^{+\infty} (\hat{v}^{1/2}(x) - v_+^{1/2})\,\mathrm{d}x\right) \text{ real.}$$

Proof. Reviewing the proof of Proposition 4.1, we find that the initial transformation T is asymptotically constant in λ as $|\lambda| \to \infty$, and thus, the projection onto the "hyperbolic" mode corresponding to the 1–1 entry has the same property. It follows that the Kato ODE $R' = (PP' - P'P)R$ used to propagate initializing bases at $\pm\infty$ (see Section 5), where P is the projection onto the stable (respectively. unstable) subspace of $A_\pm$, asymptotically decouples, yielding a constant (stable) hyperbolic basis element, and two stable and two unstable "parabolic" basis elements coming from the 4×4 lower right-hand block of matrix E further below. But, the latter decouples into what may be recognized as a pair of first-order systems corresponding to the scalar variable-coefficient heat equations $u_t = u_{xx}$ and $u_t = \nu u_{xx}$. Explicit evaluation of the Kato ODE, similar to but simpler than the treatment of Burgers' equation in [27], Appendix D, then yields that the Evans function for would be asymptotically *constant* if $A(x, \lambda)$ were identically equal to A_- for $x \leq 0$ and A_+ for $x \geq 0$. See also Remark 3.10, which yields the same result in much greater generality.

Though A is not constant for $x \gtrless 0$, the $|\lambda|$-asymptotic flow may be developed as in [37] in an asymptotic series in $\lambda^{-1/2}$ (respectively. λ^{-1}) in parabolic (respectively. hyperbolic) modes, to see that, up to an asymptotically constant factor (coming from $c(x) = O(1)$ terms in eigenvalues of various modes, through $e^{\int_{\pm\infty}^{0}(c(x)-c(\pm\infty))\,\mathrm{d}x}$), the flow from y to x is given asymptotically by $e^{\pm\lambda^{1/2}\int_y^x \nu^{-1/2}\hat{v}(z)^{1/2}\,\mathrm{d}z}$ and $e^{\pm\lambda^{1/2}\int_y^x \hat{v}(z)^{1/2}\,\mathrm{d}z}$ in parabolic

modes and $e^{-\lambda(y-x)}$ in the hyperbolic mode (note: constant rate, so no resulting correction), whence, correcting for variation in the integrand from the constant-coefficient case, we obtain (4.34).

We omit the details, referring the reader to [27, 12] and especially [37] for similar but more difficult calculations. □

Remark 4.5. *We see from* (4.34) *that the asymptotic behavior of contours is independent of shock amplitude or model parameters, being determined up to rescaling of* λ *by* sgn α. *This explains the "universal" quality of contour diagrams arising here and in* [27, 12]. *In practice, it is not necessary to compute* α, *since the knowledge that limit* (4.34) *exists allows us to determine* α, C *by curve fitting of* $\log D(\lambda) = \log C + \alpha\lambda^{1/2}$ *with respect to* $z := \lambda^{1/2}$, *for* $|\lambda| \gg 1$. *When* D *is initialized in the standard way on the real axis, so that* $\bar{D}(\lambda) = D(\bar{\lambda})$, C *is necessarily real.*

Remark 4.6. *Restricting the limiting Evans function* $D^\dagger := Ce^{\alpha\lambda^{1/2}}$ *to the imaginary axis,* $\lambda = i\tau$, $\tau \in \mathbb{R}$, *we obtain*

$$D^\dagger(i\tau) = Ce^{\alpha|\tau|^{1/2}/2}(\cos + i\sin)(\pm\alpha|\tau|^{1/2}),$$

predicting increasing winding about the origin as $\tau \to \infty$.

Since the limiting Evans function $D^\dagger := Ce^{\alpha\lambda^{1/2}}$ is nonvanishing, we may obtain practical high-frequency bounds by a convergence study on $D \to D^\dagger$, requiring, say, relative error ≤ 0.1 to obtain a conservative but reasonably sharp radius. Here, $D^\dagger$ may be estimated numerically using profile data in the formulae of Proposition 4.4, by curve-fitting as described in Remark 4.5, or, more conventionally, by numerical extrapolation in the course of the convergence study.

See, for example, the computation displayed in Figures 1–2, comparing the nonisentropic Evans function to its high-frequency limit $Ce^{\alpha\lambda^{1/2}}$ for $\Gamma = 2/3$ and $\mu = \nu = 1$, at contour radii $\Lambda = 25$ and $\Lambda = 10$, respectively, where C and α have been determined by first taking limits along the positive real axis. Clearly, convergence in both cases has already occurred, whence radius $\Lambda = 10$ is sufficient to bound unstable eigenvalues, similarly as in the isentropic case [4, 27]. By comparison (see Section 5), tracking estimates give the much more conservative bound $\Lambda = 100.4$. More extreme cases are depicted in Figures 3 and 4 for $\mu = 1$, $\nu = 5$, and gas constants $\Gamma = 2/3$ and $\Gamma = 1/5$, respectively. Note that convergence has already occurred at radius $\Lambda = 40$, which is thus sufficient to bound unstable eigenvalues; by contrast, the bounds obtained by tracking are $\Lambda = 391.3$ and $\Lambda = 1755.6$, respectively.

These figures clearly indicate the universal behavior of the high-frequency limit. This can be seen also in the contour plots of Figure 6, comparing contours for the same model and radius at different values of v_+.

Remark 4.7. *More generally, the argument of Proposition 4.34 yields*

$$D(\lambda)/e^{\alpha\lambda^{1/2}+\beta\lambda} = \text{constant}, \tag{4.36}$$

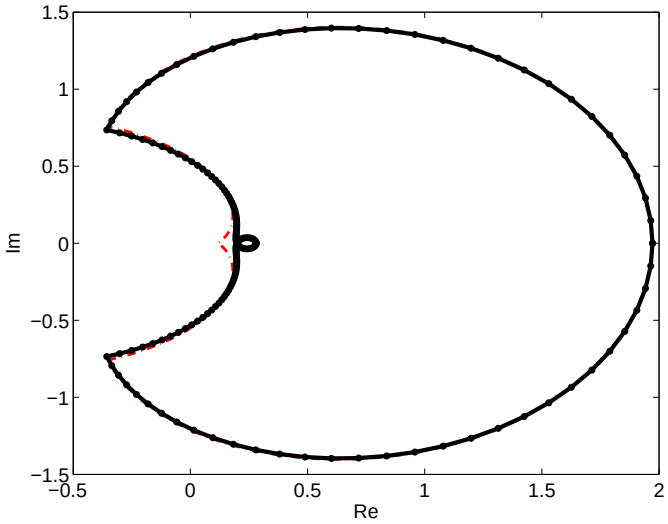

FIGURE 1. Universal behavior at high frequency: The images of the semicircle of radius 25 under the Evans function and its universal approximant (4.36) (C, α, and β determined by curve fitting), for a monatomic gas, $\Gamma = 2/3$, $\mu = \nu = 1$, in the worst case $v_+ = v_* = 1/4$. Agreement is nearly exact on the image of the outer, circular arc and most of the imaginary axis, with deviations for $|\lambda|$ small.

α and β real constants, for all hyperbolic–parabolic parabolic system of the form studied in [37, 38]*, where β corrects for variation in the rates of growth (respectively. decay) in hyperbolic modes, which are given to first order by λ times their convection rates* [37]*. That $\beta = 0$ in the present case is an accident of Lagrangian coordinates, for which hyperbolic modes are convected (in the rest frame of the shock) with the constant fluid velocity $-s$. In the more general case* (4.36)*, asymptotic behavior of contours is determined (up to rescaling in λ) by* sgn α *together with the additional parameter β/α^2.*

Remark 4.8. *Figure 4 is particularly intriguing, showing convergence also for small frequencies. This suggests the conjecture that D^* might converge identically to $D^\dagger$ in the singular limit $\Gamma \to 0$, $\nu/\mu \to \infty$ for all frequencies, small as well as large. This would be an interesting direction for further investigation. We remark that (i) the limit of D^* as $\Gamma \to 0$ is accessible by our techniques, Remark 2.2, and (ii) the limit $\nu/\mu \to \infty$ should be accessible by standard singular perturbation techniques.*

4.2. **The small-amplitude limit.** We mention in passing the following, related result noted in [27], regarding the small-amplitude limit $v_+ \to 1$.

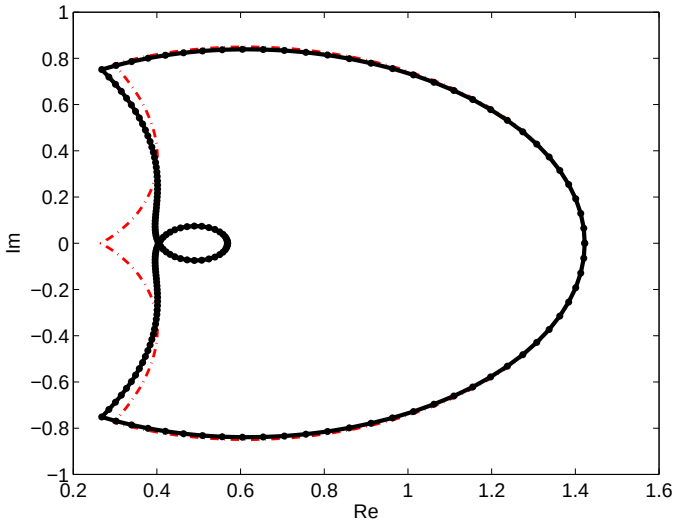

FIGURE 2. Universal behavior: The images of the semicircle of radius 10 under the Evans function and its universal approximant (4.36), for $\Gamma = 2/3$, $\mu = \nu = 1$, $v_+ = v_* = 1/4$. (Tracking radius = 100.4.)

Proposition 4.9. *The Evans function D converges uniformly as $v_+ \to 1$ on compact subsets of $\{\Re\lambda \geq 0\} \setminus \{0\}$, $\Gamma, \nu, \mu > 0$ to a constant $C(\Gamma, \nu, \mu)$.*

Proof. For $|\lambda|$ sufficiently large, this follows by Proposition 4.4 together with the fact [41] that profiles in the small-amplitude converge to an approximate Burgers equation profile given by a symmetric tanh function, for which α vanishes to order $|1-v_+|$ in (4.35). For $|\lambda|$ bounded, this follows as described in [27] by the fact that the Evans function also converges in the small-amplitude limit to the Evans function associated with the scalar, Burgers equation, which by direct calculation is constant. (The latter fact may be deduced, alternatively, by a simple scaling argument showing that, for Burgers equation, the small-amplitude limit and large-amplitude limits are equivalent.) □

The significance of Proposition 4.9 is that the exponential rate of decay of profiles to their endstates $U_\pm$ goes to zero in the characteristic limit $v_+ \to 1$, as seen in the proof of Lemma 2.3. Thus, we cannot immediately conclude as in the "regular" large-amplitude limit $v_+ \to v_*$ even that a limit exists as $v_+ \to 1$. Moreover, a second consequence is that the computational domain $[-L_-, L_+]$ on which we carry out numerical evaluation of the Evans function enlarges to $|L_\pm| \to \infty$ as $v_+ \to 1$, since this must be taken roughly proportional to the inverse of the exponential rate for numerical accuracy; see Section 5.3.3. Thus, the boundary $v_+ = 1$ is not directly accessible by

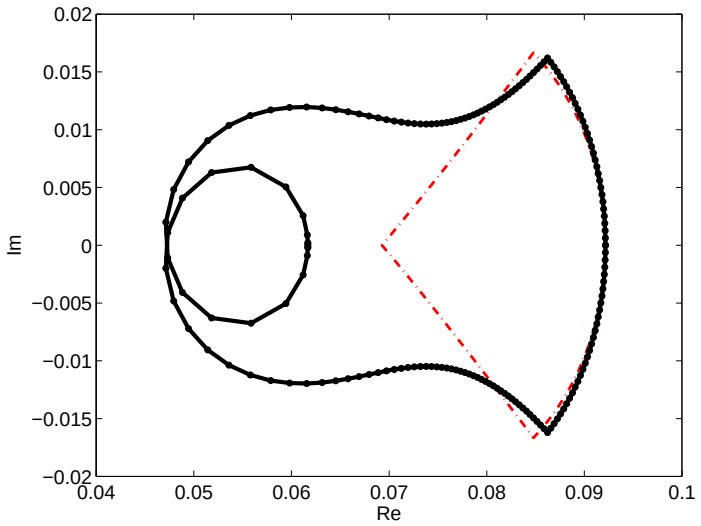

FIGURE 3. Universal behavior: The images of the semicircle of radius 40 under the Evans function and its universal approximant (4.36), for $\Gamma = 2/3$, $\mu = 1$, $\nu = 5$, $v_+ = v_* = 1/4$. (Tracking radius = 391.3.)

numerical Evans function techniques, but requires a singular-perturbation analysis, either carried out numerically or else analytically as above. Alternatively, small-amplitude instability may be ruled out by energy estimates as described in the introduction; see [39, 30, 4].

Remark 4.10. *Similarly as described just below Remark 4.6 for the high-frequency limit, the small-amplitude limit may be used to obtain a sharp but nonrigorous*[2] *lower bound on the amplitude of unstable shocks by a convergence study requiring relative error* $< 1/2$ *between Evans values and their constant limit: or, still sharper, and more conveniently estimated, to require relative error* $< 1/2$ *between the Evans function and its estimated high-frequency approximant. Convergence in the small- and large-amplitude limits* $v_+ \to 1$ *and* $v_+ \to v_*$ *is illustrated numerically in Fig. 6.*

5. Numerical protocol

We now describe the numerical algorithm, based on approximate computation of the Evans function, by which we shall locate any unstable eigenvalues, if they exist, in our system, over the compact parameter range under investigation. Specifically, using analyticity of the Evans function in $\Re\lambda \geq 0$, we numerically compute the winding number around a large semicircle $B(0,\Lambda) \cap \{\Re\lambda \geq 0\}$ enclosing all possible unstable roots, obtaining

[2] Recall that rigorous small-amplitude bounds are available by energy estimates [30, 4].

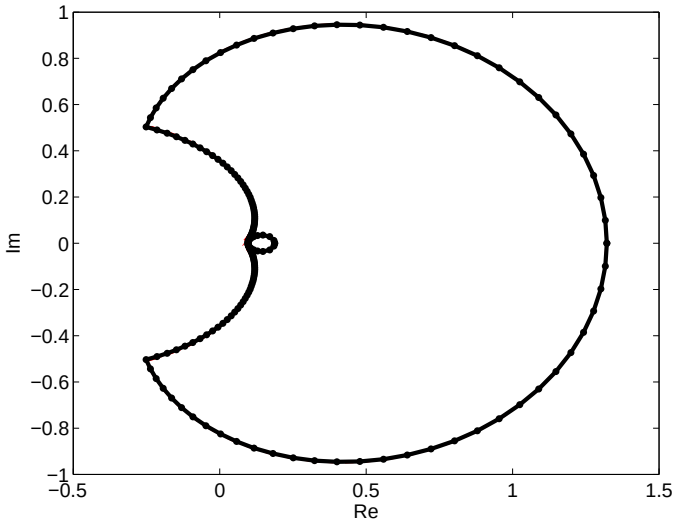

FIGURE 4. Universal behavior: The images of the semicircle of radius 40 under the Evans function and its universal approximant (4.36), for $\Gamma = 1/5$, $\mu = 1$, $\nu = 5$, $v_+ = v_* = 1/11$. (Tracking radius = 1755.6.). Note that the two curves are essentially indistinguishable, except that the universal approximate does not loop but instead cusps near the origin.

a count of the number of unstable eigenvalues within, and thus of the total number of unstable eigenvalues. This approach was first used by Evans and Feroe [14] and has been advanced further in various directions in, for example, [43, 42, 2, 6, 7, 5, 30].

5.1. **Approximation of the profile.** Following [4, 27], we compute the traveling wave profile using MATLAB's `bvp4c` routine, which is an adaptive Lobatto quadrature scheme. These calculations are performed on a finite computational domain $[-L_-, L_+]$ with projective boundary conditions $M_\pm(U - U_\pm) = 0$. The values of approximate plus and minus spatial infinity $L_\pm$ are determined experimentally by the requirement that the absolute error $|U(\pm L_\pm) - U_\pm|$ be within a prescribed tolerance $TOL = 10^{-3}$. This requirement is not too demanding in practice; we make more stringent requirements later in evaluating the Evans function.

5.2. **Bounds on unstable eigenvalues.** We next estimate numerically the coefficients $|\mathcal{F}^*_{kl}|(x,\Lambda)$ defined in (4.2), (4.1), using the numerically generated profiles described above, generating an iterative sequence $\Lambda_{j+1} := T(\Lambda_j)$,

$$T(\Lambda) := 2\max\{1,\nu\} \max_x \Big(\frac{|\mathcal{F}^*_{--}| + |\mathcal{F}^*_{++}| + 2\sqrt{|\mathcal{F}^*_{-+}||\mathcal{F}^*_{+-}|}}{\hat{v}^{1/2}}(x,\Lambda) \Big)^2.$$

	ν				
Γ	0.2	0.5	1.0	2.0	5.0
0.2	398.6	388.8	385.3	733.8	1755.6
0.4	211.7	182.3	175.1	325.0	762.0
0.6	222.5	123.4	111.5	198.4	449.8
2/3	226.8	114.3	100.4	175.3	391.3
0.8	236.5	103.9	85.3	142.6	307.1
1.0	253.8	100.8	73.7	113.8	229.2
1.2	274.3	106.6	69.7	98.7	183.1
1.4	300.8	117.5	70.5	91.6	154.9
1.6	347.4	131.8	74.5	89.8	138.0
1.8	397.3	148.7	80.8	91.8	128.6
2.0	450.3	167.5	88.7	96.7	124.7

TABLE 1. Tracking bound Λ_* vs. Γ, ν ($v_+ = v_*$).

This is easily seen to converge, with odd terms monotone increasing and even terms monotone decreasing or the reverse, to a fixed point $\Lambda_* = T(\Lambda_*)$, which, by Proposition 4.1, gives a bound $|\lambda| \leq \Lambda_*$ on the maximum modulus of unstable eigenvalues $\Re\lambda \geq 0$. Computations for a range of typical parameter values are displayed in Table 1, for the worst case $v_+ = v_*$. Note the degradation of bounds for $\nu \gg \mu$ or $\nu \ll \mu$, a consequence of multiple scales (stiffness).

Remark 5.1. *The poor rigorous tracking estimates obtained for $\nu \gg \mu$ or $\nu \ll \mu$ could in principle be improved by a refined tracking estimate separating further the parabolic modes: that is, taking account of the presence of multiple parabolic scales; see* [37, 44] *for methodology. Ultimately, this should be treated by singular perturbation techniques as in* [1]*, separating out also fast/slow behavior of the background profile.*

5.2.1. *High-frequency convergence study.* Alternatively, we could obtain more realistic, but nonrigorous unstable eigenvalue bounds by a convergence study as $|\lambda| \to \infty$, as described in Section 4.1. A convenient algorithm is to estimate coefficients C, α of the high-frequency approximant $D(\lambda) \sim Ce^{\alpha\sqrt{\lambda}}$ by linear fit of $\log D \sim \log C + \alpha\sqrt{\lambda}$ as λ goes to real positive infinity, then approximate by binary search the value Λ_* at which relative error between $D(\lambda)$ and $Ce^{\alpha\sqrt{\lambda}}$ is less than $TOL_1 = 10^{-1}$ on the positive semicircle $|\lambda| = \Lambda_*$, $\Re\lambda \geq 0$, indicating convergence to this tolerance, hence nonvanishing of D, for $|\lambda| \geq \Lambda_*$, $\Re\lambda \geq 0$. The resulting bounds are much less conservative than those obtained by rigorous tracking estimates of Section 5.2; see for example the discussion following Remark 4.6. We do not pursue this here, as our main interest is in rigorous bounds. However, the observation seems quite important for practical numerical testing, as typical

differences in radius are an order of magnitude or more, and the size of the radius appears to be the main limiting factor in computational efficiency.

5.3. **Approximation of the Evans function.** We compute the Evans functions for comparison by two rather different techniques, both of which have been demonstrated to give good numerical results.

5.3.1. *The exterior product method.* Following [6, 7, 8, 5], we work with "lifted equations"

$$\mathcal{W}' = A^{(k)}\mathcal{W}, \quad \mathcal{W} := W_1 \wedge \cdots \wedge W_k,$$

evolving subspaces encoded as exterior products of basis elements W_j, where

$$A^{(k)}(W_1 \wedge \cdots \wedge W_k) := (AW_1 \wedge \cdots \wedge W_k) + \cdots + (W_1 \wedge \cdots \wedge AW_k), \tag{5.1}$$

defining $\mathcal{W}^+$ and $\mathcal{W}^-$ as k_+- and k_--products of bases $\{W_j^+\}$ and $\{W_j^-\}$ of the subspaces of solutions of $W' = AW$ decaying at $+\infty$ and $-\infty$; in the present case, $k_+ = 3$, $k_- = 2$.

In this setting, the stable (respectively. unstable) manifold at $+\infty$ (respectively. $-\infty$) corresponds to a single solution/vector, eliminating difficulties of "parasitic modes", etc.; see [8, 30, 5, 4] for further discussion. We then compute the Evans function as

$$D(\lambda) = \mathcal{W}^+ \wedge \mathcal{W}^-|_{x=0}$$

or, alternatively, as $D(\lambda) = \tilde{\mathcal{W}}^+ \cdot \mathcal{W}^-|_{x=0}$, where $\tilde{\mathcal{W}}^+$ is an appropriate solution of the adjoint equation $\tilde{\mathcal{W}}' = -(A^{(k)})^*\tilde{\mathcal{W}}$; see [6, 7, 8, 5, 30, 4] for further details.

5.3.2. *The polar coordinate method ("analytic orthogonalization").* An alternative method proposed in [30] is to encode $\mathcal{W} = \gamma\Omega$, where "angle" $\Omega = \omega_1 \wedge \cdots \wedge \omega_k$ is the exterior product of an orthonormal basis $\{\omega_j\}$ of Span $\{W_1, \ldots, W_k\}$ evolving independently of γ by some implementation (e.g., Davey's method) of continuous orthogonalization and "radius" γ is a complex scalar evolving by a scalar ODE slaved to Ω, related to Abel's formula for evolution of a full Wronskian; see [30] for further details. This might be called "analytic orthogonalization", as the main difference from standard continuous orthogonalization routines is that it restores the important property of analyticity of the Evans function by the introduction of the radial function γ (Ω by itself is not analytic).

Advantages/disadvantages: The exterior product method is *linear*, but evolving in a high-dimensional ($\sim n^n$) space. The polar coordinate method is *nonlinear*, hence less well-conditioned and involving more complicated function calls, but evolving on a lower-dimensional manifold ($\sim n^2$). Thus, there is a tradeoff in dimensions vs. conditioning, with the polar coordinate method the only reasonable option for high-dimensional systems and the exterior product method somewhat faster and more efficient for low-dimensional systems [30]. Both methods are effective (and reasonably comparable in efficiency) for $n \leq 7$ or so.

Role as numerical check: Since the two methods involve completely different ODE, one linear and the other nonlinear, agreement in their results is strong, if indirect, evidence that equations have been properly encoded and solutions accurately approximated, *at least on the finite computational domain* $[-L_-, L_+]$. We address in the following subsection the separate question of determining appropriate $L_\pm$.

5.3.3. *Determination of approximate spatial infinities.* Denoting by $A_\pm^{(k)}(\lambda)$ the limits at $\pm\infty$ of the lifted matrix $A^{(k_\pm)}(x,\lambda)$ defined in (5.1), and μ_+ (respectively. μ_- the eigenvalue of $A_+^{(k)}$ (respectively. $A_-^{(k)}$) of smallest (respectively. largest) real part, we find that there holds a uniform bound

$$e^{(A^{(k)}-\mu)_\pm x} \leq C_*, \quad x \lessgtr 0 \tag{5.2}$$

on any compact subset of $\Re\lambda \geq 0$, for Γ bounded from zero, and μ, ν bounded and bounded from zero, for some $C_* > 0$. For λ bounded from zero, this follows by consistent splitting on $\{\Re\lambda \geq 0\} \setminus \{0\}$, and the choice of $k_\pm$ as dimensions of stable (respectively. unstable) subspaces of $A_\pm$, which together imply that, away from $\lambda = 0$, $\mu_\pm$ are simple eigenvalues of $A_\pm^{(k)}$. For λ near zero, on the other hand, we may verify directly that $\mu_\pm$ are semisimple, by the same considerations used to verify continuous extension of stable (respectively, unstable) subspaces of $A_\pm$: simple in the case of μ_-, since the unstable subspace remains uniformly spectrally separated from remaining eigenvalues of A_-; semisimple in the case of μ_+, because hyperbolic characteristics a_j^+ are simple, and thus eigenvalues μ_j^+ of small real part, by the standard theory of [17, 56, 37], are analytic and semisimple, of form $\mu_j^+ \sim -\lambda/a_j^+$, whence μ^+ (the sum of the $k_+ = 3$ eigenvalues of largest real part) is semisimple as well.

Applying the "quantitative gap lemma" of Theorem C.2, [4], we have therefore that the relative error between the solution $\mathcal{W}^\pm(\pm L_\pm)$ at plus or minus approximate spatial infinity $x = \pm L_\pm$ and the constant-coefficient initialization $\mathcal{V}^\pm e^{\mu_\pm \pm L_\pm}$ is bounded by $\frac{\epsilon}{1-\epsilon}$, for

$$\epsilon := C_* |A^{(k)}(\cdot,\lambda) - A_\pm^{(k)}(\lambda)|_{L^1(\pm L, \pm\infty)}. \tag{5.3}$$

Using the bound $|M^{(k)}| \leq k|M|$ established in Appendix E, and the asymptotic behavior

$$A_j(x,\lambda) - A_{j,\pm}(\lambda) \approx Q_j e^{-\theta_\pm |x|}, \tag{5.4}$$

$A =: \lambda A_1 + A_0$ for $x \to \pm\infty$, we may thus estimate

$$\begin{aligned}
\max_{|\lambda|\le\Lambda} |A^{(k)}(\cdot,\lambda) - A_\pm^{(k)}(\lambda)|_{L^1(\pm L,\pm\infty)} &\le \max_{|\lambda|\le\Lambda} k|A(\cdot,\lambda) - A_\pm(\lambda)|_{L^1(\pm L,\pm\infty)} \\
&\approx \max_{|\lambda|\le\Lambda} \frac{k|A(\pm L_\pm,\lambda) - A_\pm(\lambda)|}{\theta_\pm} \\
&\le k\frac{|A_0(\pm L_\pm) - A_{0,\pm}| + \Lambda|A_1(\pm L_\pm) - A_{1,\pm}|}{\theta_\pm} \\
&= k\frac{|A(\pm L_\pm,0) - A_\pm(0)|}{\theta_\pm} \\
&\quad + k\frac{|A(\pm L_\pm,\Lambda) - A_\pm(\Lambda) - (A(\pm L_\pm,0) - A_\pm(0))|}{\theta_\pm}.
\end{aligned}$$

This gives a theoretical relative error bound of TOL (tolerance) between initializing basis at $\pm L$ and actual basis for the theoretical Evans function, provided that

$$\begin{aligned}
&C_* k\Big(\frac{|A(\pm L_\pm,0) - A_\pm(0)|}{\theta_\pm} + \frac{|A(\pm L_\pm,\Lambda) - A_\pm(\Lambda) - (A(\pm L_\pm,0) - A_\pm(0))|}{\theta_\pm}\Big) \\
&\quad \le \frac{TOL}{1+TOL} \approx TOL,
\end{aligned}$$

or, approximately,

$$\begin{aligned}
&|A(\pm L_\pm,0) - A_\pm(0)| + |A(\pm L_\pm,\Lambda) - A_\pm(\Lambda) - (A(\pm L_\pm,0) - A_\pm(0))| \\
&\quad \le \frac{\theta_\pm}{C_* k} TOL.
\end{aligned} \tag{5.5}$$

Remark 5.2. *Alternatively, working directly from* (5.4)*, we may solve* (5.5) *with equality for*

$$L_\pm \approx \frac{\log C_* + \log k + \log(|Q_0^\pm| + \Lambda|Q_1^\pm|) + \log\theta_\pm^{-1} + \log TOL^{-1}}{\theta_\pm}. \tag{5.6}$$

A reasonably good bound (noting insensitivity of log, and also cancellation in large λ vs. small θ effects) for $k = 2$, $\Lambda \sim 10^2$, $TOL = 10^{-3}$, $|Q_1| = 1$ for the sparse matrix Q_1, $C_* = 10^2$, and throwing out θ and $|Q_0|$ terms as negligible for large $|\lambda|$, is

$$L_\pm \approx \frac{\log 2 + 7\log 10}{\theta_\pm} \approx \frac{17}{\theta_\pm}.$$

Numerical algorithm Starting with the values needed for accurate profile approximation, we increment $L_\pm$ by some fixed step-size (here, we have chosen step-size 5) until (5.5) is satisfied, taking $k = 2$, $TOL = 10^{-3}$, and conservatively estimating $C_* = 10^2$. In Table 2, we have displayed values of $\theta_\pm$, $L_\pm$ computed from (5.5) with $TOL = 10^{-3}$, $C_* = 10^2$, for various values of Γ and v_+, with $\mu = 1$ and ν set to the value $\nu = (3/4)\frac{9\gamma-5}{4}$, $\gamma = \Gamma + 1$, predicted by the kinetic theory of gases; see Appendix B. In principle, C_*

$v_+ = 0.7$						
Γ	L_-	θ_-	$17/\theta_-$	L_+	θ_+	$17/\theta_+$
0.2	68	0.28	61	68	0.27	61
0.4	75	0.26	67	74	0.26	67
0.6	83	0.23	74	81	0.23	74
2/3	85	0.22	76	83	0.23	76
0.8	90	0.21	81	87	0.22	81
1.0	98	0.20	87	92	0.21	87
$v_+ = v_*$						
Γ	L_-	θ_-	$17/\theta_-$	L_+	θ_+	$17/\theta_+$
0.2	22	0.91	19	24	0.83	19
0.4	28	0.70	25	27	0.71	25
0.6	34	0.57	30	31	0.61	30
2/3	36	0.53	32	33	0.59	32
0.8	41	0.48	36	36	0.54	36
1.0	47	0.41	42	40	0.48	42

TABLE 2. $L_+(\theta_+)/L_-(\theta_-)$ vs. Γ, v_+.

could be estimated numerically for a more precise bound. In practice, convergence studies reveal these bounds to be rather conservative; see Table 3, or [4, 27] in the isentropic case.

Translation to $x = 0$. The above-described algorithm is designed to achieve relative accuracy TOL of $\mathcal{W}_\pm$ at $x = \pm L_\pm$, whereas the accuracy of the Evans function is determined, rather, by their relative errors at $x = 0$. A complete description of the error must thus include also a discussion of possible magnification through the evolution from $\pm L_\pm$ to 0. However, as discussed in [6, 7], the flow toward $x = 0$ is in fact quite stable, since, by construction, the modes $\mathcal{W}_\pm$ we seek to approximate are the fastest decaying in the flow toward infinity, hence the fastest growing in backward flow toward zero, with all other modes decaying exponentially in relative size. Thus, in practice, the resulting magnification in error is negligible; see [6, 7] for further discussion or numerical studies.

Remark 5.3. *Since the polar coordinate method computes the same quantity $\mathcal{W}$ in different coordinates, the initialization error bounds derived for the exterior product method apply also for the polar coordinate method and so the same values $L_\pm$ may be used for both computations.*

5.3.4. *ODE protocol.* Following [6, 7, 8, 5, 30, 4], to further improve the numerical efficiency and accuracy of the shooting scheme, we rescale $\mathcal{W}$ and $\widetilde{\mathcal{W}}$ to remove exponential growth/decay at infinity, and thus eliminate potential problems with stiffness. Specifically, we let $\mathcal{W}(x) = e^{\mu^- x}\mathcal{V}(x)$, where μ^- is the growth rate of the unstable manifold at $x = -\infty$, and we

L	rel($\widetilde{W}^+(0)$)	rel($W^-(0)$)	rel(D)
20	2.2(-2)	5.8(-3)	3.8(-3)
25	3.3(-3)	8.8(-4)	4.6(-4)
30	4.7(-4)	1.3(-4)	5.3(-5)
35	6.4(-5)	1.8(-5)	5.7(-6)
40	8.7(-6)	2.6(-6)	8.9(-7)
45	1.1(-6)	3.5(-7)	2.2(-7)

TABLE 3. Convergence of $\widetilde{W}^+(0)$, $W^-(0)$, and D as L increases from 25 to 50, incrementing by 5, for a diatomic gas ($\gamma = 7/5$ and $\nu/\mu = 1.47$. The values were computed for a quarter circle of radius $R = 69$ consisting of 90 points. Relative errors were computed at each point and the maximum value along the contour is reported with the next higher value of L being the baseline.

solve instead

$$\mathcal{V}'(x) = (A^{(k)}(x,\lambda) - \mu^- I)\mathcal{V}(x).$$

We initialize $\mathcal{V}(x)$ at $x = -\infty$ to be the eigenvector of $A_-^{(k)}(\lambda)$ corresponding to μ^-. Similarly, it is straightforward to rescale and initialize $\widetilde{\mathcal{W}}(x)$ at $x = +\infty$. To produce analytically varying Evans function output, the initial data $\mathcal{V}(-L_-)$ and $\widetilde{\mathcal{V}}(L_+)$ must be chosen analytically using (3.12). The algorithm of [8] works well for this purpose, as discussed further in [4, 30].

The ODE calculations for individual λ are carried out using MATLAB's `ode45` routine, which is the adaptive 4th-order Runge-Kutta-Fehlberg method (RKF45), after scaling out the exponential decay rate of the constant-coefficient solution at spatial infinity, as described just above. This method is known to have excellent accuracy [5, 30]; in addition, the adaptive refinement gives automatic error control. Typical runs involved roughly 300 mesh points per side, with error tolerance set to `AbsTol = 1e-6` and `RelTol = 1e-8`.

5.4. **Winding number computation.** We compute the winding number for fixed parameter values about the semicircle $\partial\{\lambda : \Re\lambda \geq 0, |\lambda| \leq \Lambda\}$ by varying values of λ along 180 points of the contour, with mesh size taken quadratic in modulus to concentrate sample points near the origin where angles change more quickly, and summing the resulting changes in $\arg(D(\lambda))$, using $\Im \log D(\lambda) = \arg D(\lambda) (\mathrm{mod} 2\pi)$, available in MATLAB by direct function calls. As a check on winding number accuracy, we test a posteriori that the change in argument of D for each step is less than $\pi/8$. Recall, by Rouché's Theorem, that accuracy is preserved so long as the argument varies by less than π along each mesh interval.

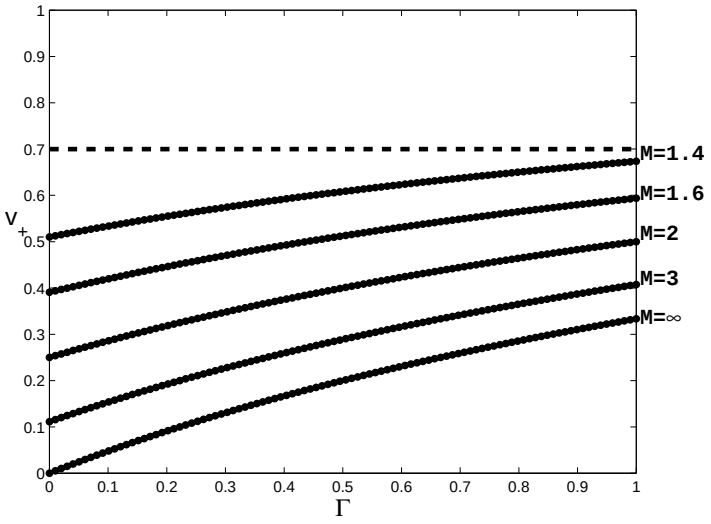

FIGURE 5. Iso-Mach curves in Γ, v_+.

6. Numerical results

Finally, we describe our numerical results in various cases, using the numerical method just described, varying v_+ between .7 and the theoretical lower value v_* in our rescaled coordinates (2.12). For comparison between these and standard coordinates, it is useful to convert these values to their associated *Mach number*, a standard dimensionless measure of shock strength discussed further in Appendix D. As computed in (D.1), this is given by $M = \frac{\sqrt{2}}{\sqrt{(\Gamma+2)(v_+ - v_*)}}$, which for $1 - v_+$ small reduces using (2.33) to

$$M = \frac{1}{\sqrt{1 - (1-v_+)\frac{2+\Gamma}{2}}} \approx 1 + (1-v_+)\frac{2+\Gamma}{4} \leq 1 + |1 - v_+|$$

for the range $\Gamma \in [0, 2]$ under consideration. In particular, for the upper limit $v_+ = .7$ of our computations, we have on the reduced range $0 \leq \Gamma \leq 1$ the exact upper bound $M \leq (.55)^{-1/2}$, or approximately Mach 1.35, well within the small-amplitude regime. Recall that stability of small-amplitude shocks has been shown analytically in [29].

The smallest computed physical value $v_+ - v_* = 10^{-3}$ corresponds to Mach $M \sim 100$, at which we see already convergence of the Evans function to that of the nonphysical limit $v_+ = v_*$, corresponding to Mach $M = \infty$. For a visual comparison, we display iso-Mach (constant Mach number) curves in the Γ-v_+ plane in Figure 5.

6.1. **Description of experiments: broad range.** In the main case considered, of μ and ν of comparable but wide-ranging size, a first set of experiments was carried out in the range $\Gamma \in [.2, 2]$, $\nu \in [0.2, 5]$, sampling at mesh points

$$(\Gamma, \nu) \in \{0.2, 0.4., 0.6, 2/3, 0.8, 1.0, 1.2, 1.4, 1.6, 1.8, 2.0\} \times \{0.2, 0.5, 1.0, 2.0, 5.0\},$$

55 pairs in all, where, for each value (Γ, ν), v_+ was varied among 8 mesh points on a logarithmic scale from .7 to v_*, for a total of 440 runs in all. In each of the cases that we examined, the winding number was zero, indicating spectral stability and thereby nonlinear stability and existence of shock layers in the vanishing viscosity limit, by the results of [38, 54, 22, 23, 24]. These runs took 12 days to complete, of which 8 days were spent on the upper extreme case $\nu = 5$, and 2 days were spent on the lower extreme case $\nu = .2$, both out of physical range.

6.2. **Description of experiments: physical range.** A second set of experiments was carried out for Γ values corresponding to monatomic, diatomic, etc. gas on a refined mesh for ν within the smaller, physical range $\nu \in [1, 2]$ indicated by Appendices A and B, sampling at

$$(\Gamma, \nu) \in \{2/11, 2/9, 2/7, 2/5, 2/3\} \times \{1.0, 1.1, 1.2, 1.3, 1.4, 1.5, 1.6, 1.7, 1.8, 1.9, 2.0\},$$

with v_+ again varied among 8 mesh points on a logarithmic scale from .7 to v_*, again a total of 440 runs. The results again were winding number zero for each case tested, indicating spectral stability. These runs took 10 days to complete. We remark that runs for $\nu = 5$ and $\nu = .2$ took over twice as long to complete compared with the average, again reflecting the stiffness alluded to in Remark 5.1, associated with difference in scale between ν and $\mu = 1$.

Appendix A. Gas constants for air

In this appendix, we list the various relevant gas constants for dry air at normal temperatures and pressures. For the specific gas constant (universal gas constant $R \approx 8.3 \frac{\text{J}}{\text{moles}\cdot\text{K}}$ divided by molar mass), we have

$$\bar{R} \approx 287.05 \, \frac{\text{J}}{\text{kg} \cdot \text{K}},$$

J = Joules, kg = Kilograms, K = degrees Kelvin [10]. For specific heat at constant volume, we have

$$c_v \approx 716 \, \frac{\text{J}}{\text{kg} \cdot \text{K}}$$

at 0 °C (degrees Celsius) [50]. Computing the dimensionless quantity $\Gamma = \bar{R}/c_v$, we thus obtain

$$\Gamma \approx 0.401,$$

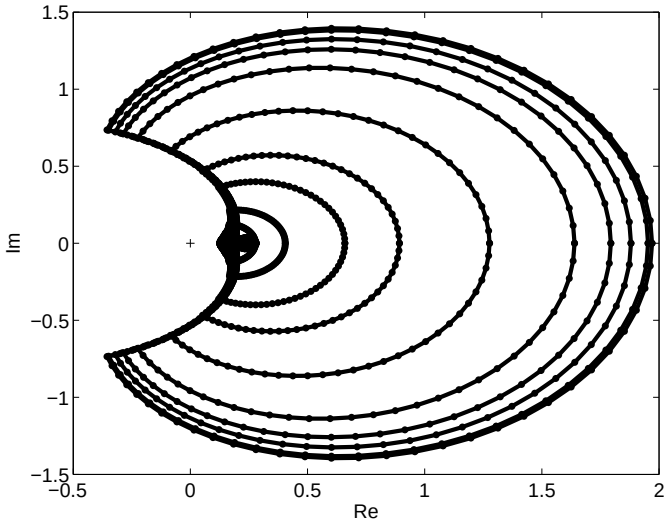

FIGURE 6. Convergence to the limiting Evans function as $v_+ \to v_*$ for a monatomic gas, $\Gamma = 2/3$, $\mu = \nu = 1$, $v_* = 1/4$. The contours depicted, going from inner to outer, are images of the semicircle of radius 25 under the Evans function D for $v_+ = .7, .6, .5, .4, .35, .3, .27, .26, .255, .251, .2501$. The outermost contour is the image under the limiting Evans function D^*, which is essentially indistinguishable from the images for $v_+ = .251$ and $v_+ = .2501$.

in remarkable agreement with the value $\Gamma = .4$ predicted by statistical mechanical approximation $\Gamma = \frac{2}{2n+1}$ for a diatomic gas, $n = 2$. (Recall that air is composed of roughly 78% nitrogen, 21% oxygen, and 1% neon, so it is essentially a diatomic mixture.)

For thermal conductivity, the ratio of heat flux to temperature gradient asserted by Fourier's law of heat conduction, we have the value

$$\kappa \approx .025 \, \frac{\mathrm{W}}{\mathrm{m} \cdot \mathrm{K}},$$

W = Watts = Joules per second, and for dynamic or "first" viscosity, the rate of proportionality of shear stress to velocity gradient of a shear flow asserted in Newton's law of viscosity, the value

$$\mu_1 \approx (1.78) \times 10^{-5} \, \frac{\mathrm{kg}}{\mathrm{m} \cdot \mathrm{s}}.$$

m = meters, s = seconds [10, 52]. Collecting these values, we may compute the "constant-volume Prandtl number"

$$\mathrm{Pr}_v := c_v \mu_1 / \kappa \approx \frac{(716)(1.78) \times 10^{-5}}{(.025)} \approx .510, \tag{A.1}$$

or very nearly 1/2. This is related to the usual (constant-pressure) Prandtl number $\mathrm{Pr} := c_p\mu_1/\kappa$ by $\mathrm{Pr}_v = \mathrm{Pr}/\gamma$, where $\gamma := c_p/c_v$ is the heat capacity ratio, or *adiabatic index*, relating specific heat at constant pressure c_p to specific heat at constant volume c_v, under ideal gas assumptions, $\gamma = 1+\Gamma$. For a variety of gases over a fairly wide range of temperatures [52, p. 43], $\mathrm{Pr} \approx 0.7$.

Recall that the effective viscosity appearing in the one-dimensional Navier–Stokes equations is $\mu = 2\mu_1 + \mu_2$, the sum of twice the dynamic viscosity and the "second viscosity" μ_2, which is commonly taken as $\mu_2 = -(2/3)\mu_1$ based on the assumption that pressure equals "mean pressure" defined as one-third the trace of the three-dimensional stress tensor, an approximation that appears to be in good agreement with experiment at least for monatomic and diatomic gases [3, 45]. We therefore take $\mu \approx (4/3)\mu_1$, giving

$$\nu/\mu = (3/4)\mathrm{Pr}_v^{-1} \approx 1.47. \tag{A.2}$$

Interesting values for computation are thus $\Gamma = .4$ ($\gamma = 1.4$), $\nu/\mu = 1.47$, modeling air.

Remark A.1. *A convenient alternative formula involving commonly tabulated dimensionless quantities is*

$$\nu/\mu = (3/4)\gamma\mathrm{Pr}^{-1}, \tag{A.3}$$

where Pr *denotes (usual) Prandtl number and* $\gamma = c_p/c_v$ *the adiabatic index. Assuming the value* $\mathrm{Pr} \approx 0.7$ *typical of simple (e.g., monatomic, diatomic) gases, we obtain the general rule of thumb*

$$\nu/\mu \approx (1.09)\gamma; \tag{A.4}$$

see Table 4 for more precise values.

Remark A.2. *We note also the alternative formula*

$$\Gamma = \left(\frac{c_p}{\bar{R}} - 1\right)^{-1}$$

for the Gruneisen constant in terms of specific heat at constant pressure. (For air, $c_p \approx 1\,\mathrm{J/g\cdot K} = 1,000\,\mathrm{J/kg\cdot K}$.*)*

Appendix B. Gas constants for other gases

B.1. **Ideal Gases.** Using the dimensionless formula (A.3), we next investigate typical parameter values for some common gases. For an ideal gas, the Prandtl number is predicted by *Eucken's formula* [9]

$$\mathrm{Pr} = \frac{4\gamma}{9\gamma - 5}, \tag{B.1}$$

giving in combination with (A.3) the simple relation

$$\nu/\mu = (3/4)\frac{9\gamma - 5}{4}. \tag{B.2}$$

Gas	γ (th.)	Pr (th.)	Pr (exp.)	ν/μ (th.)	ν/μ (exp.)	rel. err.
He	5/3	.667	.694	1.88	1.80	4%
Ar			.669		1.87	.05%
H_2	7/5	.737	.712	1.43	1.47	2%
N_2			.735		1.43	0%
O_2			.732		1.43	0%
CO			.763		1.38	3.5%
CO_2	4/3	.762	.819	1.31	1.22	6.8%
H_2S			.929		1.08	17.6%
SO_2			.833		1.17	10.7%
CH_4	5/4	.8	.777	1.17	1.28	9.5%

TABLE 4. Theoretical vs. experimental values of Pr and ν/μ and relative error in ν/μ at $20\,^\circ\mathrm{C} = 68\,^\circ\mathrm{F}$ (room temperature).

We display in Table 4 the relation for various gases between the theoretical value (B.1) and experimentally measured values for Pr (Table 1.9-1 of [9], adapted from [35], p. 250). Though not displayed, experimental values of the adiabatic index $\gamma = c_p/c_v$ match theoretical predictions to within 1% for monatomic and diatomic gases, 3% for triatomic, and 4.8% for five-atomic gas CH_4, as do experimental values vs. theoretical predictions of the Gruneisen coefficient $\Gamma = \bar{R}/c_v$.

In summary, the equation of state and temperature law predicted by ideal gas theory appear to be extremely accurate at usual temperatures, while the predictions involving viscosity (μ, Pr, κ) degrade with molecular complexity, being nearly exact for monatomic gases, quite good for most diatomic gases, but only a first approximation for triatomic and more complicated gases. Indeed, the derivation of viscosity and heat conduction formulae involves additional simplifying assumptions whose validity degrades with structural complexity [9]. *Thus, we may use with some confidence the theoretical prediction* (B.2) *for simple gases, but must consult experimental data for complex gases.*

Remark B.1. *From* (2.7) *and* (B.1) *we obtain the theoretical range*

$$\gamma \in [1, 1.66...], \quad \nu/\mu \in [.75, 1.88].$$

B.2. **Temperature dependence and the kinetic theory of gases.** Though the ratio (B.1) of viscosity and heat conductivity predicted by the kinetic theory of gases is constant, the absolute size predicted for either one depends on temperature, T. For example, the predicted viscosity for a

monatomic gas obtained through Chapman–Enskog expansion of the Boltzmann equations with hard-sphere potential is *Chapman's formula*

$$\mu_1 = \mu_1(T) = (2/3)\sqrt{\frac{mkT}{\pi\sigma^2}}, \tag{B.3}$$

where m is mass per particle in kilograms kg, k is the Boltzmann constant in Joules per degrees Kelvin J/K, T is temperature in degrees Kelvin K, and σ is the collision cross section in meters squared m^2, given approximately by one-half diameter squared [3, 9]. This appears to give good physical agreement, and a refined version given by *Sutherland's formula*

$$\mu_1 = \frac{(1+\tilde{m})T^{3/2}}{T+\tilde{m}}, \tag{B.4}$$

$\tilde{m}$ constant, to give extraordinarily good agreement [9]. More generally, viscosity is typically modeled by

$$\mu_1 = CT^q, \quad 1/2 \le q \le 1, \tag{B.5}$$

with $q \approx .76$ for air [36].

Properly, we should include the above-described temperature-dependence in the physical study of large-amplitude shock layers. Though beyond the scope of the present project, this appears to be feasible by a slight modification of the same techniques, as we discuss further in Appendix F.

Appendix C. Liquids and dense gases

For comparison, values of the Prandtl number Pr for various media at 20 °C are [52, p. 80]:

- around 0.024 for mercury,
- around 0.7 for air and helium,
- around 7 for water,
- around 16 for ethyl alcohol,
- around 10,000 for castor oil, and
- around 12,000 for glycerin.

The adiabatic index (specific heat ratio) of water is $\gamma \approx 1.01 \approx 1.0$, hence

$$\nu/\mu = \gamma/\mathrm{Pr} \approx \mathrm{Pr}^{-1} \approx .143,$$

quite far from the gas values of Table 4.

Moreover, for dense gases or liquids, the ideal gas assumptions break down, and the polytropic equation of state (2.6) must be replaced by more sophisticated versions such as Peng–Robinson or "stiffened polytropic" equations of state [26, 25]. For example, water is often modeled by a stiffened equation of state

$$p = \Gamma\rho e - \gamma P_0 \tag{C.1}$$

behaving like a prestressed material, with base stress P_0 and Γ determined empirically: for example, $\gamma \sim 6.1$ and

$$P_0 = 2,000\,\mathrm{MPa} = 2 \times 10^9\,\mathrm{N/m^2} = 2 \times 10^9\,\mathrm{kg/m \cdot s^2}$$

or $\gamma = 7.42$ and $P_0 = 296.2\,\mathrm{MPa}$ [32, 25]. Similar techniques are used to model liquid argon, nickel, mercury, etc. [26, 11].

It would be very interesting to investigate the effects on stability of these modifications in the polytropic equation of state. For the moment, what we can say, physically, is that *insofar as they conform to a polytropic (ideal gas) equation of state, shock waves are stable*. However, above a critical density, even standard, simple (e.g., monatomic or diatomic) gases are observed *not* to conform to a polytropic law [13], and in this regime our mathematical conclusions hold no sway.

Appendix D. Computation of the Mach number

A dimensionless quantity measuring shock strength is the *Mach number*

$$M = \frac{u_- - \sigma}{c_-}$$

(for a left-moving shock), where u_- is the downwind velocity, σ is the shock speed, and c_- is the downwind sound speed, all in Eulerian coordinates. The conservation of mass equation in Eulerian coordinates is $\rho_t + (\rho u)_x = 0$, giving jump condition $\sigma[\rho] = [\rho u]$, or, in Lagrangian coordinates,

$$\sigma = \frac{u_+ v_- - u_- v_+}{v_- - v_+}.$$

Thus,

$$M = \frac{u_- - \sigma}{c_-} = \frac{v_-(u_- - u_+)}{c_-(v_- - v_+)} = \frac{v_-[u]}{c_-[v]} = -s\frac{v_-}{c_-},$$

which, under our normalization $s = -1$, $v_- = 1$, gives

$$M = c_-^{-1} = (\Gamma(1+\Gamma)e_-)^{-1/2}$$

or, using $e_- = \frac{(\Gamma+2)(v_+ - v_*)}{2\Gamma(\Gamma+1)}$,

$$M = \frac{\sqrt{2}}{\sqrt{(\Gamma+2)(v_+ - v_*)}}. \tag{D.1}$$

In the strong-shock limit $v_+ \to v_*$, $M \sim (v_+ - v_*)^{-1/2}$; in the weak shock limit $v_+ \to 1$, $M \to 1$.

Appendix E. Lifted Matrix bounds

We establish the following useful bound on the operator norm of the "lifted" matrix $A^{(k)}$ acting on k-exterior products $V = V_1 \wedge \cdots \wedge V_k$ by the operation

$$A^{(k)}V := AV_1 \wedge \cdots \wedge V_k + \cdots + V_1 \wedge \cdots \wedge AV_k.$$

induced by a given matrix A, where $A^{(k)}$ by convention is represented with respect to standard basis elements $e_{j_1} \wedge \cdots e_{j_k}$.

Lemma E.1. *In the matrix operator norm $|\cdot|_p$ with respect to ℓ^p,*

$$|A^{(k)}|_p \leq k|A|_p, \quad 1 \leq p \leq \infty. \tag{E.1}$$

Proof. It is sufficient to establish (E.1) for $p = 1$ and $p = \infty$, the result for other p following from the Riesz–Thorin interpolation theorem

$$|M|_p \leq |M|_{s_1}^{\theta_1} |M|_{s_2}^{\theta_2},$$

$\theta_j > 0$, $\theta_1 + \theta_2 = 1$, for $s_1 < p < s_2$.

The ℓ^1 operator norm is equal to the maximum over all columns of the sum of moduli of column entries, or, equivalently, the maximum ℓ^1 norm of the image of a standard basis element. Applying this definition to $A^{(k)}$), we find readily that the ℓ^1 norm of the image of a standard basis element is bounded by the sum of the ℓ^1 norms of k terms of form

$$Ae_{j_1} \wedge \cdots \wedge e_{j_k},$$

expanded in standard exterior product basis elements. As each of these clearly has ℓ^1 norm bounded by the ℓ^1 norm of Ae_{j_1}, and thus by $|A|_1$, we obtain the result for $p = 1$. The result for $p = \infty$ may be obtained by duality, using $(A^{(k)})^* = (A^*)^{(k)}$ together with $|M|_\infty = |M^*|_1$. □

Appendix F. Temperature-dependent viscosity

Finally, we discuss the changes needed to accommodate a common temperature or other dependence in the coefficients of viscosity and heat conduction. For concreteness, we focus on the case

$$\mu(e) = \mu_* e^q, \quad \kappa(e) = \nu_* e^q, \qquad 0 \leq q \leq 1, \tag{F.1}$$

μ_*, ν_* constant, encompassing the Chapman formula (B.3) predicted by the kinetic theory of gases as well as the more general formula (B.5), indicating afterward by a few brief remarks the extension to more general situations.

F.1. **Rescaling.** Under (2.5), (F.1), it is easily checked that the Navier–Stokes equations are invariant under the modified rescaling

$$(x, t, v, u, T) \to (-\epsilon s|\epsilon s|^{-2q} x, \epsilon s^2 |\epsilon s|^{-2q} t, v/\epsilon, -u/(\epsilon s), T/(\epsilon^2 s^2)), \tag{F.2}$$

consisting of (2.12) with x and t rescaled by the common factor $|\epsilon s|^{-2q}$. For the Chapman viscosity $q = 1/2$, this reduces to

$$(x, t, v, u, T) \to (-(\text{sgn } s)x, |s|t, v/\epsilon, -u/(\epsilon s), T/(\epsilon^2 s^2)), \tag{F.3}$$

essentially undoing the rescaling in the x-coordinate. Evidently, the Rankine-Hugoniot analysis of Section 2.4 goes through unchanged.

F.2. **Profile equations.** The profile equations (2.24)–(2.25) are unaffected by dependence of μ, κ. Setting $\nu_* := \kappa_*/c_v$, and making the change of independent variable

$$\frac{\mathrm{d}x}{\mathrm{d}y} = \mu = \mu_* e^q, \tag{F.4}$$

we may thus reduce them to the form

$$v' = \frac{1}{\mu_*}\left[v(v-1) + \Gamma(e - ve_-)\right], \tag{F.5}$$

$$e' = \frac{v}{\nu_*}\left[-\frac{(v-1)^2}{2} + (e - e_-) + (v-1)\Gamma e_-\right] \tag{F.6}$$

already treated in the constant-viscosity case, $' = \frac{d}{dy}$. To obtain the profile in original x-coordinates, we have only to recover the change of coordinates $x = x(y)$ by solving (F.4) with $e = \hat{e}(y)$, $\hat{e}$ the constant-viscosity profile.

Recalling that $\hat{e}(y) = e_\pm + O(e^{-\theta|y|})$, $\theta > 0$ for $y \gtrless 0$, where $e_+ > 0$ and $e_- > 0$ except in the strong-shock limit $v_+ \to v_*$, we find that x and y are equivalent coordinates on $x > 0$, and on $x < 0$ are equivalent for v_+ bounded from the strong-shock limit v_*. However, in the strong-shock limit $v_+ = v_*$, $e_- = 0$, we have the interesting phenomenon that the $x < 0$ part of the shock profile terminates at a finite value $X_- = x(-\infty)$, since

$$|x(-\infty)| = |\int_0^{-\infty} (e(y)/c_v)^q \,\mathrm{d}y| \leq C\int_0^{-\infty} e^{-q\theta|y|}\,\mathrm{d}y < +\infty.$$

Remark F.1. *Holding $(v,u,e)_-$ fixed, and varying v_+ toward its minimum value v_*, we find that*

$$s = \sqrt{-[p]/[v]} \to \infty$$

as $p_+ \sim e_+ \sim (e_+/e_-) \sim (v_+ - v_*)^{-1}$, since v_+ is bounded from zero, e_- is being held constant, and ratio e_+/e_- is independent of scaling so may be computed from formulae (2.34)–(2.35)*. Thus, shock width in the constant-viscosity case is of order $|v_+ - v_*|$ going to zero as shock strength (measured in specific volume v) goes to its maximum value of $|1 - v_*|$. By comparison, for the Chapman viscosity $\mu \sim e^{1/2}$, the shock width remains approximately constant in the strong-shock limit, a significant deviation in the theories. See, e.g.,* [51, 26] *for further discussion of this and related points.*

Remark F.2. *Clearly, the same procedure may be used to determine profiles for arbitrary $\mu = \mu(v,u,e)$, κ/μ constant, setting $\frac{\mathrm{d}x}{\mathrm{d}y} = \mu(v,u,e)$ in* (F.4).

F.2.1. *Limiting behavior.* The limiting profile equations at $v_+ = v_*$ are

$$v' = \frac{1}{\mu_*}\left[v(v-1) + \Gamma e\right], \tag{F.7}$$

$$e' = \frac{v}{\nu_*}\left[-\frac{(v-1)^2}{2} + e\right]. \tag{F.8}$$

Linearizing about U_- gives

$$\begin{pmatrix} v \\ e \end{pmatrix}' = M \begin{pmatrix} v \\ e \end{pmatrix}, \qquad M := \begin{pmatrix} \mu_*^{-1} & \Gamma\mu_*^{-1} \\ 0 & \nu_*^{-1} \end{pmatrix}. \tag{F.9}$$

For $\nu_*/\mu_* > 1$, we have, therefore, that the slow unstable manifold at $-\infty$ is tangent to $(\Gamma(\nu_*/\mu_*)/(1-(\nu_*/\mu_*)), 1)$, with growth rate $\sim e^{-\nu_*^{-1}y}$, and thus generically

$$\frac{\hat e_y}{\hat e} \sim \frac{1}{\nu_*}, \quad \frac{\hat u_y}{\hat e} = \frac{\hat v_y}{\hat e} \sim \frac{\Gamma/\mu_*}{1-\nu_*/\mu_*} \quad \text{as } y \to -\infty. \tag{F.10}$$

For $\nu_*/\mu_* < 1$, the slow manifold is tangent to $(1,0)$, and we have the opposite situation that, generically, $\frac{\hat e_y}{\hat e} \sim \mu_*^{-1}$, $\frac{\hat u_y}{\hat e} \to \pm\infty$ as $y \to -\infty$.

F.3. **Eigenvalue equations.** Computing the linearized integrated eigenvalue equations as in Section 3.1, and making the change of variables (F.4), we obtain after some rearrangement, the modified, temperature-dependent equations

(F.11)

$$\lambda\hat\mu v + v' - u' = 0,$$

$$\lambda\hat\mu u + \Big[1 + \frac{q\hat e_y}{\hat e\hat v} - \frac{q\hat u_y^2}{\hat\mu\hat e\hat v}\Big]u' + \Big[\frac{\Gamma}{\hat v} - \frac{q\hat u_y}{\hat e\hat v}\Big]\epsilon' + \frac{\Gamma\hat u_y}{\hat v}u + \left[-\frac{\Gamma\hat e}{\hat v^2} + \frac{\hat u_y}{\hat v^2}\right]v' = \frac{u''}{\hat v},$$

$$\lambda\hat\mu\epsilon + \epsilon' + \left[\hat u_y - \frac{\nu_*\hat u_{yy}}{\hat v}\right]u + \left[\frac{\Gamma\hat e}{\hat v} - (\nu_*+1)\frac{\hat u_y}{\hat v} - \frac{q\nu_*\hat u_y\hat e_y}{\hat\mu\hat e\hat v}\right]u' + \left[\frac{\nu_*\hat e_y}{\hat v^2}\right]v' = \frac{\nu_*}{\hat v}\epsilon'',$$

$' = \frac{\mathrm{d}}{\mathrm{d}y}$, where $(\hat v, \hat u, \hat e) = (\hat v, \hat u, \hat e)(y)$ are just as in the constant-viscosity case.

This yields a first-order eigenvalue system

$$W' = A(y,\lambda)W, \tag{F.12}$$

(F.13)

$$A(y,\lambda) = \begin{pmatrix} 0 & 1 & 0 & 0 & 0 \\ \lambda\hat\mu\nu_*^{-1}\hat v & \nu_*^{-1}\hat v & \nu_*^{-1}\hat v\hat u_y - \hat u_{yy} & \lambda\hat\mu g(\hat U) & g(\hat U) - h(\hat U) \\ 0 & 0 & 0 & \lambda\hat\mu & 1 \\ 0 & 0 & 0 & 0 & 1 \\ 0 & \Gamma - \frac{q\hat u_y}{\hat e} & \lambda\hat\mu\hat v + \Gamma\hat u_y & \lambda\big(\hat\mu\hat v - \frac{q\hat u_y^2}{\hat e}\big) & f(\hat U) - \lambda\hat\mu \end{pmatrix},$$

$$W = (\epsilon, \epsilon', u, v, v')^T, \quad ' = \frac{d}{dy}, \tag{F.14}$$

where

$$\begin{aligned} f(\hat U) &:= \frac{\hat u_y - \Gamma\hat e}{\hat v} + \hat v\Big(1 + \frac{q\hat e_y}{\hat e\hat v} - \frac{q\hat u_y^2}{\hat\mu\hat e\hat v}\Big) \\ &= 2\hat v - 1 - \Gamma e_- + \Big(\frac{q\hat e_y}{\hat e} - \frac{q\hat u_y^2}{\hat\mu\hat e}\Big), \end{aligned} \tag{F.15}$$

$$g(\hat{U}) := \nu_*^{-1}\Big(\Gamma\hat{e} - (\nu_* + 1)\hat{u}_y\Big) - \frac{q\hat{u}_y\hat{e}_y}{\hat{\mu}\hat{e}\hat{v}}, \tag{F.16}$$

$$h(\hat{U}) := -\frac{\hat{e}_y}{\hat{v}} = -\nu_*^{-1}\left(-\frac{(\hat{v}-1)^2}{2} + (\hat{e} - e_-) + (\hat{v}-1)\Gamma e_-\right), \tag{F.17}$$

$$\hat{\mu} := \hat{e}^q, \tag{F.18}$$

reducing for $q = 0$ to that of the constant-viscosity case. We omit the details, which are straightforward but tedious.

Noting that all terms not appearing in the constant-viscosity case involve derivatives of the profile, hence vanish at $y = \pm\infty$ so long as $e_\pm$ (appearing in denominators) do not vanish, we may conclude by the constant-viscosity analysis consistent splitting away from the strong-shock limit $v_+ \to v_*$, $e_- \to 0$. We may thus construct an Evans function that is analytic in λ and continuous in all parameters away from the strong-shock limit.

F.3.1. *Limiting behavior.* Assume, as for the physical cases considered above, that

$$\nu/\mu \equiv \nu_*/\mu_* > 1. \tag{F.19}$$

Then, by the limiting analysis (F.10), all terms in $A(y,\lambda)$ *remain bounded and well-defined in the strong-shock limit.* Thus, we may hope for convergence as in the constant-viscosity case.

On the other hand, new terms $\hat{e}_y/\hat{e}$, $\hat{u}_y/\hat{e}$ of order

$$\frac{\hat{e} - e_-}{\hat{e}} = 1 - \frac{e_-}{\hat{e}}$$

exhibit singular behavior in the $v_+ \to v_*$, $e_- \to 0$ limit reminiscent of that of the isentropic case [27]. In particular, since $e_-/\hat{e}$ approaches its limiting value 1 as $y \to -\infty$ only as $|\hat{e} - e_-|/e_-$, this means that $|A - A_\pm|$ does not decay at uniform exponential rate as $y \to -\infty$, but only as $O(e_-^{-1}e^{-\theta|y|})$, $\theta > 0$, so that the strong-shock limit is a singular perturbation in the sense of [44, 27] and not a regular perturbation as in the constant-viscosity case. Thus, an analysis of behavior in the strong-shock limit is likely to involve a delicate boundary-layer analysis similar to that of [27] in the isentropic case. This appears to be a very interesting direction for further investigation.

Remark F.3. *The appearance of condition* (F.19) *is unexpected, dividing into two cases the physical behavior in the strong-shock limit.*

Remark F.4. *Our numerical experiments, though still quite preliminary (restricted to diatomic gas,* $\Gamma = .4$, $\nu_*/\mu_* = 1.43$, $q = 0.5$*) so far again indicate unconditional stability, also in the temperature-dependent case.*

F.4. **General dependence.** We conclude by discussing briefly the case of general, possibly inhomogeneous dependence of viscosity on (v, u, T). The homogeneous case goes exactly as before, working in y-coordinates and noting Remark F.2 and the discussion of Section F.3.

The inhomogeneous case is well-illustrated by Sutherland's formula (B.4). Fixing a left-hand state (the "true" strong-shock limit), without loss of generality $v_- = 1$, and taking $v_+ \to v_*$, rescale by (F.2) with $q = 1/2$ and $\epsilon = 1$, $s = s(v_+)$. The result *in the rescaled coordinates* is

$$\mu = (4/3)s^{-1}\frac{(1+\tilde{m})(s^2T)^{3/2}}{(s^2T)+\tilde{m}} = (4/3)\frac{(1+\tilde{m})T^{3/2}}{T+s^{-2}\tilde{m}}, \tag{F.20}$$

converging in the strong-shock limit $v_+ \to v_*$, $s \sim |v_+ - v_*|^{-1} \to \infty$ to the homogeneous Chapman formula

$$\mu = (4/3)(1+\tilde{m})T^{1/2}.$$

Other inhomogeneous laws go similarly, converging in the strong-shock limit in each case to an appropriate homogeneous law. Thus, *inhomogeneous dependence poses no essential new difficulty.*

References

[1] J. Alexander, R. Gardner, and C. Jones. A topological invariant arising in the stability analysis of travelling waves. *J. Reine Angew. Math.*, 410:167–212, 1990.

[2] J. C. Alexander and R. Sachs. Linear instability of solitary waves of a Boussinesq-type equation: a computer assisted computation. *Nonlinear World*, 2(4):471–507, 1995.

[3] G. K. Batchelor. *An introduction to fluid dynamics*. Cambridge Mathematical Library. Cambridge University Press, Cambridge, paperback edition, 1999.

[4] B. Barker, J. Humpherys, K. Rudd, and K. Zumbrun. Stability of viscous shocks in isentropic gas dynamics. (Preprint, 2007).

[5] T. J. Bridges, G. Derks, and G. Gottwald. Stability and instability of solitary waves of the fifth- order KdV equation: a numerical framework. *Phys. D*, 172(1-4):190–216, 2002.

[6] L. Q. Brin. *Numerical testing of the stability of viscous shock waves.* PhD thesis, Indiana University, Bloomington, 1998.

[7] L. Q. Brin. Numerical testing of the stability of viscous shock waves. *Math. Comp.*, 70(235):1071–1088, 2001.

[8] L. Q. Brin and K. Zumbrun. Analytically varying eigenvectors and the stability of viscous shock waves. *Mat. Contemp.*, 22:19–32, 2002. Seventh Workshop on Partial Differential Equations, Part I (Rio de Janeiro, 2001).

[9] W. B. Brower. *A Primer in Fluid Mechanics: Dynamics of Flows in One Space Dimension.* CRC Press, 1999.

[10] W. B. Brower. *Theory, Tables, and Data for Compressible Flow.* Hemisphere Publishing, 1990.

[11] F. Cirak, R. Deiterding, and S. P. Mauch, Large-scale fluid-structure interaction simulation of viscoplastic and fracturing thin-shells subjected to shocks and detonations. *Comput. & Structures*, 85:1049–1065, 2007.

[12] N. Costanzino, J. Humpherys, T. Nguyen, and K. Zumbrun, Spectral stability of noncharacteristic boundary layers of isentropic Navier–Stokes equations. (Preprint, 2007).

[13] M. S. Cramer. Nonclassical dynamics of classical gases. In *Nonlinear Waves in Real Fluids*, pp. 91-145. Springer, 1991.
[14] J. W. Evans and J. A. Feroe. Traveling waves of infinitely many pulses in nerve equations. *Math. Biosci.*, 37:23–50, 1977.
[15] H. Freistühler and P. Szmolyan. Spectral stability of small shock waves. *Arch. Ration. Mech. Anal.*, 164(4):287–309, 2002.
[16] H. Freistühler and P. Szmolyan. Spectral stability of small-amplitude viscous shock waves in several dimensions. (Preprint, 2007).
[17] R. A. Gardner and K. Zumbrun. The gap lemma and geometric criteria for instability of viscous shock profiles. *Comm. Pure Appl. Math.*, 51(7):797–855, 1998.
[18] R. Gardner and C.K.R.T. Jones. A stability index for steady state solutions of boundary value problems for parabolic systems. *J. Differential Equations.*, 91(2):181–203, 1991.
[19] R. Gardner and C.K.R.T. Jones. Traveling waves of a perturbed diffusion equation arising in a phase field model. *Indiana Univ. Math. J.* 38(4):1197–1222, 1989.
[20] F. Gesztesy, Y. Latushkin, and K.A. Makarov. Evans Functions, Jost Functions, and Fredholm Determinants. *Arch. Ration. Mech. Anal.*, to appear.
[21] D. Gilbarg, The existence and limit behavior of the one-dimensional shock layer. *Amer. J. Math.* 73:256–274, 1951.
[22] O. Guès, G. Métivier, M. Williams, and K. Zumbrun. Navier–Stokes regularization of multidimensional Euler shocks. *Ann. Sci. École Norm. Sup.* 39(4):75–175, 2006.
[23] O. Guès, G. Métivier, M. Williams, and K. Zumbrun. Viscous boundary value problems for symmetric systems with variable multiplicities. (Preprint, 2006).
[24] O. Guès, G. Métivier, M. Williams, and K. Zumbrun. Nonclassical multidimensional viscous and inviscid shocks. To appear, *Duke Math. J.*, 2007.
[25] K. K. Haller, Y. Ventikos, D. Poulikakos, and P. Monkewitz. Computational study of high-speed liquid droplet impact. *J. Appl. Phys.*, 92(5):2821–2828, Sept 2002.
[26] W. G. Hoover. Structure of a shock-wave front in a liquid. *Phys. Rev. Lett.*, 42(23):1531–1534, Jun 1979.
[27] J. Humpherys, O. Lafitte, and K. Zumbrun. Stability of viscous shock profiles in the high Mach number limit. (Preprint, 2007).
[28] J. Humpherys, G. Lyng, and K. Zumbrun. Multidimensional spectral stability of large-amplitude Navier–Stokes shocks. (In preparation).
[29] J. Humpherys and K. Zumbrun. Spectral stability of small-amplitude shock profiles for dissipative symmetric hyperbolic-parabolic systems. *Z. Angew. Math. Phys.*, 53(1):20–34, 2002.
[30] J. Humpherys and K. Zumbrun. An efficient shooting algorithm for Evans function calculations in large systems. *Phys. D*, 220(2):116–126, 2006.
[31] J. Humpherys, B. Sandstede, and K. Zumbrun. Efficient computation of analytic bases in Evans function analysis of large systems. *Numer. Math.*, 103(4):631–642, 2006.
[32] D. Igra and K. Takayama. Experimental and numerical study of the initial stages in the interaction process between a planar shock wave and a water column (Preprint).
[33] T. Kato. *Perturbation theory for linear operators.* Classics in Mathematics. Springer-Verlag, Berlin, 1995. Reprint of the 1980 edition.
[34] Y. Shizuta and S. Kawashima. On the normal form of the symmetric hyperbolic-parabolic systems associated with the conservation laws. *Tohoku Math. J.*, 40:449–464, 1988.
[35] L. B. Loeb. *The kinetic theory of gases.* Dover, New York, New York, USA, 1934.
[36] V. C. Liu, On the separation of gas mixtures by suction of the thermal diffusion boundary layer. *Quart. J. Mech. Appl. Math.*, VII, 1957.
[37] C. Mascia and K. Zumbrun. Pointwise Green function bounds for shock profiles of systems with real viscosity. *Arch. Ration. Mech. Anal.*, 169(3):177–263, 2003.

[38] C. Mascia and K. Zumbrun. Stability of large-amplitude viscous shock profiles of hyperbolic-parabolic systems. *Arch. Ration. Mech. Anal.*, 172(1):93–131, 2004.
[39] A. Matsumura and K. Nishihara. On the stability of travelling wave solutions of a one-dimensional model system for compressible viscous gas. *Japan J. Appl. Math.*, 2(1):17–25, 1985.
[40] G. Métivier and K. Zumbrun. Large viscous boundary layers for noncharacteristic nonlinear hyperbolic problems. *Mem. Amer. Math. Soc.*, 175(826):vi+107, 2005.
[41] R. Pego. Stable viscosities and shock profiles for systems of conservation laws. *Trans. Amer. Math. Soc.*, 282:749–763, 1984.
[42] R. L. Pego, P. Smereka, and M. I. Weinstein. Oscillatory instability of traveling waves for a KdV-Burgers equation. *Phys. D*, 67(1-3):45–65, 1993.
[43] R. L. Pego and M. I. Weinstein. Eigenvalues, and instabilities of solitary waves. *Philos. Trans. Roy. Soc. London Ser. A Math. Phys. Eng. Sci.*, 340(1656):47–94, 1992.
[44] R. Plaza and K. Zumbrun. An Evans function approach to spectral stability of small-amplitude shock profiles. *Discrete Contin. Dyn. Syst.*, 10:885-924, 2004. (Preprint, 2002).
[45] L. Rosenhead. A discussion on the first and second viscosities of fluids. *Proc. Roy. Soc. London Ser. A Math. Phys. Eng. Sci.*, 226(1164):1–6, 1954.
[46] J. Smoller. *Shock waves and reaction-diffusion equations*. Springer-Verlag, New York, second edition, 1994.
[47] D. Serre. *Systems of conservation laws. 1*. Cambridge University Press, Cambridge, 1999. Hyperbolicity, entropies, shock waves, Translated from the 1996 French original by I. N. Sneddon.
[48] D. Serre. *Systems of conservation laws. 2*. Cambridge University Press, Cambridge, 2000. Geometric structures, oscillations, and initial-boundary value problems, Translated from the 1996 French original by I. N. Sneddon.
[49] M. Slemrod. Dynamic phase transitions in a van der Waals fluid. *J. Differential Equations*, 52(1):1–23, 1984.
[50] V. V. Sychev, A. A. Vasserman, A. D. Kozlov, G. A. Spiridonov, and V. A. Tsymarny. *Thermodynamic Properties of Air*. National Standard Reference Data Service of the USSR: A Series of Property Tables, Hemisphere Publishing, 1987.
[51] C. Truesdell. The present status of the controversy regarding the bulk viscosity of fluids. *Proc. of the Royal Soc. of London, Series A Math. Phys. Eng. Sci.*, 226(1164):59–65, 1954.
[52] F. M. White. *Viscous Fluid Flow*. 2nd ed., McGraw-Hill, 1991.
[53] K. Zumbrun. Planar stability criteria for multidimensional viscous shock waves. *CIME lecture notes, Cetraro, Italy 2003*, Preprint (2003) (95 pp.); to appear, CIME research notes, Springer (2007).
[54] K. Zumbrun. Stability of large-amplitude shock waves of compressible Navier-Stokes equations. In *Handbook of mathematical fluid dynamics. Vol. III*, pages 311–533. North-Holland, Amsterdam, 2004. With an appendix by Helge Kristian Jenssen and Gregory Lyng.
[55] K. Zumbrun. Dynamical stability of phase transitions in the p-system with viscosity-capillarity. *SIAM J. Appl. Math.* 60(6):1913–1924, 2000.
[56] K. Zumbrun and P. Howard. Pointwise semigroup methods and stability of viscous shock waves. *Indiana Univ. Math. J.*, 47(3):741–871, 1998.
[57] K. Zumbrun and D. Serre. Viscous and inviscid stability of multidimensional planar shock fronts. *Indiana Univ. Math. J.*, 48 (1999) 937–992.

Department of Mathematics, Brigham Young University, Provo, UT 84602
E-mail address: jeffh@math.byu.edu

Department of Mathematics, University of Wyoming, Laramie, WY 82071
E-mail address: glyng@uwyo.edu

Department of Mathematics, Indiana University, Bloomington, IN 47402
E-mail address: kzumbrun@indiana.edu